SCIENCE AND PROJECT PLANNING FOR THE FORWARD PHYSICS FACILITY IN PREPARATION FOR THE 2024–2026 EUROPEAN PARTICLE PHYSICS STRATEGY UPDATE

Jyotismita Adhikary,[1] Luis A. Anchordoqui,[2] Akitaka Ariga,[3,4] Tomoko Ariga,[5] Alan J. Barr,[6] Brian Batell,[7] Jianming Bian,[8] Jamie Boyd,[9] Matthew Citron,[10] Albert De Roeck,[9] Milind V. Diwan,[11] Jonathan L. Feng,[8] Christopher S. Hill,[12] Yu Seon Jeong,[13] Felix Kling,[14] Steven Linden,[11] Toni Mäkelä,[8] Kostas Mavrokoridis,[15] Josh McFayden,[16] Hidetoshi Otono,[5] Juan Rojo,[17,18] Dennis Soldin,[19] Anna Stasto,[20] Sebastian Trojanowski,[1] Matteo Vicenzi,[11] and Wenjie Wu[8]

on behalf of the FPF Working Groups

[1] *National Centre for Nuclear Research, Pasteura 7, Warsaw, PL-02-093, Poland*
[2] *Department of Physics and Astronomy, Lehman College,*
City University of New York, Bronx, NY 10468, USA
[3] *Albert Einstein Center for Fundamental Physics, Laboratory for High Energy Physics,*
University of Bern, Sidlerstrasse 5, CH-3012 Bern, Switzerland
[4] *Department of Physics, Chiba University, 1-33 Yayoi-cho Inage-ku, Chiba, 263-8522, Japan*
[5] *Kyushu University, Nishi-ku, 819-0395 Fukuoka, Japan*
[6] *Department of Physics, University of Oxford, OX1 3RH, United Kingdom*
[7] *Department of Physics and Astronomy, University of Pittsburgh, Pittsburgh, PA 15217, USA*
[8] *Department of Physics and Astronomy, University of California, Irvine, CA 92697-4575, USA*
[9] *CERN, CH-1211 Geneva 23, Switzerland*
[10] *Department of Physics and Astronomy, University of California, Davis, CA 95616, USA*
[11] *Brookhaven National Laboratory, Upton, NY 11973, USA*
[12] *Department of Physics, The Ohio State University, Columbus, OH 43210, USA*
[13] *Department of Physics and Astronomy, University of Iowa, Iowa City, IA 52246, USA*
[14] *Deutsches Elektronen-Synchrotron DESY, Notkestr. 85, 22607 Hamburg, Germany*
[15] *University of Liverpool, Liverpool L69 3BX, United Kingdom*
[16] *Department of Physics & Astronomy, University of Sussex,*
Sussex House, Falmer, Brighton, BN1 9RH, United Kingdom
[17] *Department of Physics and Astronomy, VU Amsterdam, 1081 HV Amsterdam, The Netherlands*
[18] *Nikhef Theory Group, Science Park 105, 1098 XG Amsterdam, The Netherlands*
[19] *Department of Physics and Astronomy, University of Utah, Salt Lake City, UT 84112, USA*
[20] *Department of Physics, Penn State University, University Park, PA 16802, USA*

The recent direct detection of neutrinos at the LHC has opened a new window on high-energy particle physics and highlighted the potential of forward physics for groundbreaking discoveries. In the last year, the physics case for forward physics has continued to grow, and there has been extensive work on defining the Forward Physics Facility and its experiments to realize this physics potential in a timely and cost-effective manner. Following a 2-page Executive Summary, we present the status of the FPF, beginning with the FPF's unique potential to shed light on dark matter, new particles, neutrino physics, QCD, and astroparticle physics. We summarize the current designs for the Facility and its experiments, FASER2, FASERν2, FORMOSA, and FLArE, and conclude by discussing international partnerships and organization, and the FPF's schedule, budget, and technical coordination.

EXECUTIVE SUMMARY

High-energy colliders have enabled many groundbreaking discoveries since they were first constructed 70 years ago. As the latest example, the Large Hadron Collider (LHC) at CERN has been the center of attention in particle physics for decades. Despite this, the physics potential of the LHC is far from being fully explored, because the large detectors at the LHC are blind to collisions that produce particles in the forward direction, along the beamline. These forward collisions are a treasure trove of physics, providing the only way to study TeV neutrinos produced in the lab and unique opportunities to discover and study dark matter and other new particles beyond the Standard Model of particle physics.

The Forward Physics Facility (FPF) is a proposal to build a new underground cavern at CERN to house a suite of forward experiments during the High-Luminosity LHC (HL-LHC) era. These experiments will cover the blind spots of the existing LHC detectors and are required if the LHC is to fully realize its physics potential. The physics program of the FPF is broad and deep; see Fig. 1. The FPF can discover a wide variety of new particles that cannot be discovered at fixed target facilities or other LHC experiments. In the event of a discovery, the FPF, with other experiments, will play an essential role in determining the precise nature of the new physics and its possible connection to the dark universe. In addition, the FPF is the only facility that will be able to detect millions of neutrinos with TeV energies, enabling precision probes of neutrino properties for all three flavors. These neutrinos will also sharpen our understanding of proton and nuclear structure, enhancing the power of new particle searches at ATLAS and CMS, and enabling IceCube, Auger, KM3NeT and other astroparticle experiments to make the most of the new era of multi-messenger astronomy.

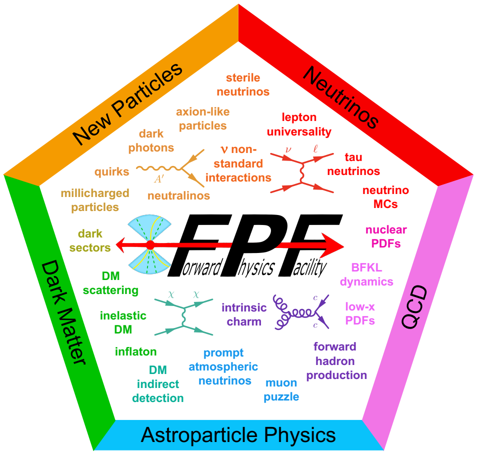

FIG. 1. The rich physics program at the FPF spans many topics and frontiers.

The Facility: An extensive site selection study has been conducted by the CERN Civil Engineering group. The resulting site is shown in Fig. 2. This location is shielded from the ATLAS interaction point (IP) by over 200 m of concrete and rock, providing an ideal location to search for rare processes and very weakly interacting particles. Vibration, radiation, and safety studies have shown that the FPF can be constructed independently of the LHC without interfering with LHC operations. A core sample, taken along the location of the 88 m-deep shaft to provide information about the geological conditions, has confirmed that the site is suitable for construction. Studies of LHC-generated radiation have concluded that the facility can be safely accessed with appropriate controls during beam operations. Flexible, safe access will allow the construction and operation of FPF experiments to be fully independent of the LHC, greatly simplifying schedules and budgets. In fact, experiments can be constructed and modified in the cavern while the LHC beam is on and other experiments are taking data, allowing a flexible program that can respond quickly to the latest developments and discoveries in particle physics and beyond.

The Experiments: The FPF is uniquely suited to explore physics in the forward region because it will house a diverse set of experiments based on different detector technologies and optimized for particular physics goals. The proposed experiments are shown in Fig. 2 and include

- FASER2, a magnetic tracking spectrometer, designed to search for light and weakly-interacting

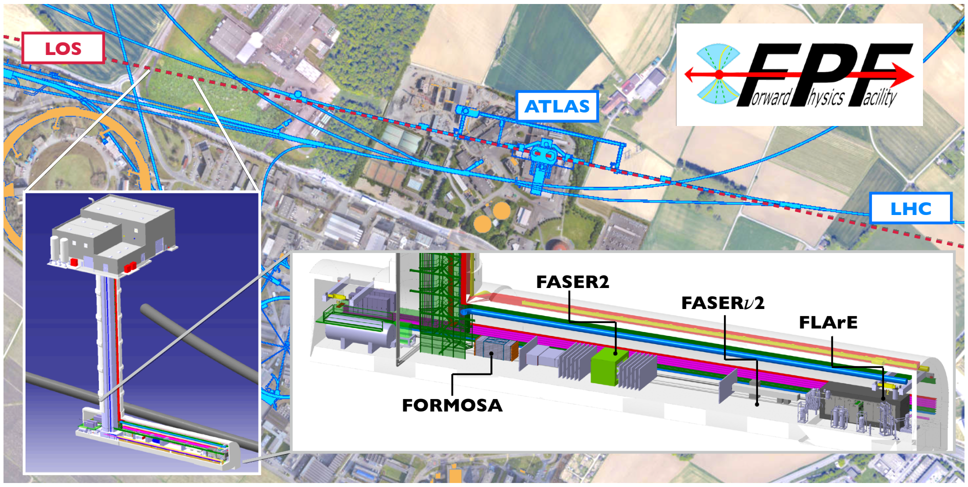

FIG. 2. The FPF is located 627–702 m west of the ATLAS IP along the line of sight. The FPF cavern is 75 m long and 12 m wide and will house a diverse set of experiments to fully explore the forward region.

states, including new force carriers, sterile neutrinos, axion-like particles, and dark sector particles, and to distinguish ν and $\bar{\nu}$ charged current scattering in the upstream detectors.

- FASERν2, an on-axis emulsion detector, with pseudorapidity range $\eta > 8.4$, that will detect $\sim 10^6$ neutrinos at TeV energies with unparalleled spatial resolution, including several thousands of tau neutrinos, among the least studied of all the known particles.
- FLArE, a 10-ton-scale, noble liquid, fine-grained time projection chamber that will detect neutrinos and search for light dark matter with high kinematic resolution, wide dynamic range and good particle-identification capabilities.
- FORMOSA, a detector composed of scintillating bars, with world-leading sensitivity to millicharged particles across a large range of masses.

Cost and Timeline: All of the planned experiments are relatively small, low cost, require limited R&D, and can be constructed in a timely way. A Class 4 cost estimate for the Facility by the CERN engineering and technical teams is 35 MCHF for the construction of the new shaft and cavern. Cost estimates for the experiments range from 2 MCHF for FORMOSA to 15 MCHF for FASERν2, as detailed in this report. The FPF requires no modifications to the LHC and will support a sustainable experimental program, without additional power consumption for the beam beyond the existing LHC program.

To fully exploit the forward physics opportunities, which will disappear for several decades if not explored in the 2030s, the FPF and its experiments should be ready for physics in the HL-LHC era as early as possible in Run 4. A possible timeline is for the FPF to be built during Long Shutdown 3 from 2026-29, the support services and experiments to be installed starting in 2029, and the experiments to begin taking data during Run 4. All of the experiments will be supported by international collaborations, and, as the physics program begins in LHC Run 4 from 2030-33, after HL-LHC upgrades are completed, the FPF will attract a large and diverse global community. In addition, as a mid-scale project composed of smaller experiments that can be realized on short and flexible timescales, the FPF will provide a multitude of scientific and leadership opportunities for junior researchers, who can make important contributions from construction to data analysis in a single graduate student lifetime. Such a timeline is guaranteed to produce exciting physics results through studies of very high-energy neutrinos, QCD, and other topics, and will additionally enhance the HL-LHC's potential for groundbreaking discoveries for many years to come.

I. PHYSICS AT THE FPF

The science case for the FPF has been developed in several dedicated FPF meetings [1–8]. The opportunities have been summarized in a 80-page review [9] and a more comprehensive 430-page White Paper [10], written and endorsed by 400 physicists.

As illustrated in Fig. 3, the FPF physics program encompasses a broad set of searches for novel new physics and unique Standard Model (SM) measurements that leverage the diverse capabilities of the suite of FPF experiments. On the side of new physics searches, this includes long-lived-particle decays to visible final states that can be probed at FASER [11], dark matter (DM) scattering signatures that can be probed at FLARE [12], and unconventional ionization caused by new particles with fractional electric charge, which can be seen at FORMOSA [13]. The SM measurements leverage the unprecedented flux of collider neutrinos that can be observed by FLArE and FASERν2 to study lepton flavor universality and non-standard interactions in the neutrino sector, probe QCD dynamics in novel kinematic regions, and resolve outstanding conundrums in astroparticle physics.

In the following, we present a few highlights of this broad program. Comprehensive discussions of the physics potential of the FPF can be found in Refs. [9, 10].

A. Dark Matter

The DM puzzle stands out as one of the foremost motivations for beyond-the-SM (BSM) physics. The form of DM realized in nature is unknown, and there are well-motivated possibilities that can only be probed by experiments at the FPF.

A generic and compelling possibility is that DM is part of a dark sector, feebly coupled to the SM by a mediator particle via a portal interaction. In this scenario, the DM relic abundance can be produced through simple thermal freeze-out, extending the traditional WIMP production

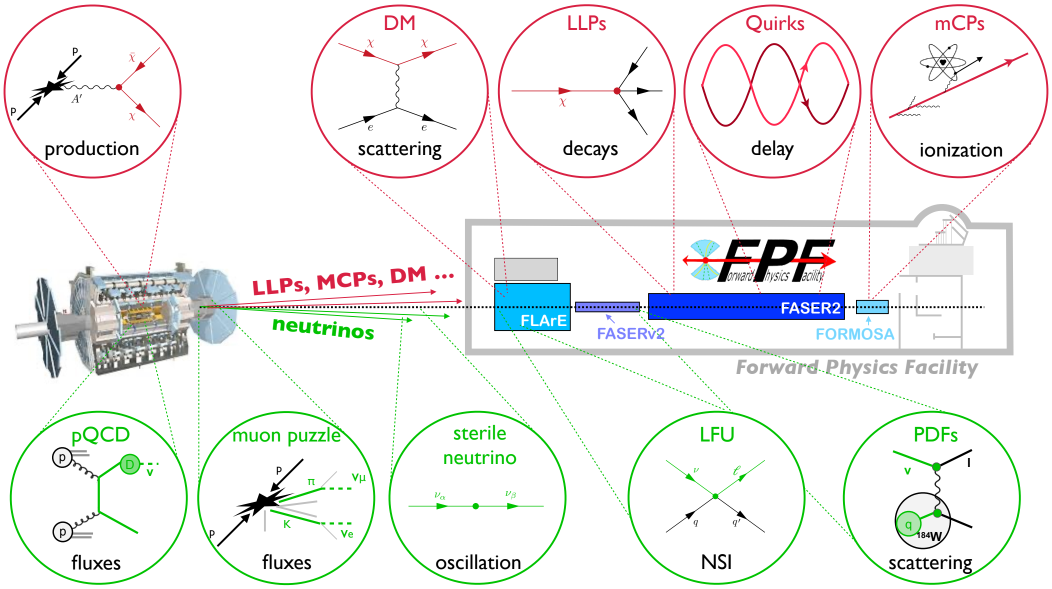

FIG. 3. **New particle searches and neutrino measurements at the FPF.** Representative examples of DM and other new particles that can be discovered and studied at the FPF (top) and of some of the many topics that will be illuminated by TeV-energy neutrino measurements at the FPF (bottom).

mechanism to DM masses in the MeV to GeV range. Such light DM, along with the associated mediator particles and other dark sector states, can be copiously produced in the forward region at the LHC, thus providing key experimental targets for BSM searches at the FPF. The search strategies required to probe these scenarios at the FPF depend on the structure of the dark sector and its mass spectrum, and we highlight a few possibilities in the following.

Mediators to DM: If the mediator is the lightest state in the dark sector, it will decay back to SM particles through the portal interaction. Due to the feebleness of this coupling, the mediators can easily possess a macroscopic decay length, thus manifesting at the FPF as a visibly-decaying long-lived particle. The powerful capability of the FPF to search for a broad spectrum of long-lived particles has been established in a large number of publications and summarized in Ref. [10]. Notably, this includes all of the benchmarks models discussed in the context of the Physics Beyond Colliders initiative [16]: dark photons, dark Higgs, heavy neutral leptons, and axion-like particles. It is worth emphasizing that in the event of a long-lived particle discovery, multiple experiments with complementary experimental capabilities will be required to determine the fundamental properties of the new state (i.e., its mass, lifetime, spin, and couplings) and its possible connection to the dark universe, and the FPF experiments will play an essential role in this endeavor.

Inelastic DM: In addition, there are also well-motivated DM scenarios featuring a rich dark sector structure that can be uniquely probed at the FPF. This is nicely illustrated in Fig. 4, which shows the expected sensitivity of FASER2 to two realisations of inelastic DM (iDM). This model contains an excited dark sector state that decays into a somewhat lighter DM particle plus a visible final state. The left panel considers a relatively heavy iDM scenario with masses in the tens of GeV range [14]. Such states are beyond the kinematic threshold of beam dump experiments, but the high energies available at the LHC imply significant production rates, and the sensitivity of the FPF to highly-displaced decays allows it to uniquely explore new regions of parameter space beyond the reach of the existing large LHC detectors. The right panel considers a case with a very small mass splitting between the excited state and the DM [15]. Due to the large particle energies in

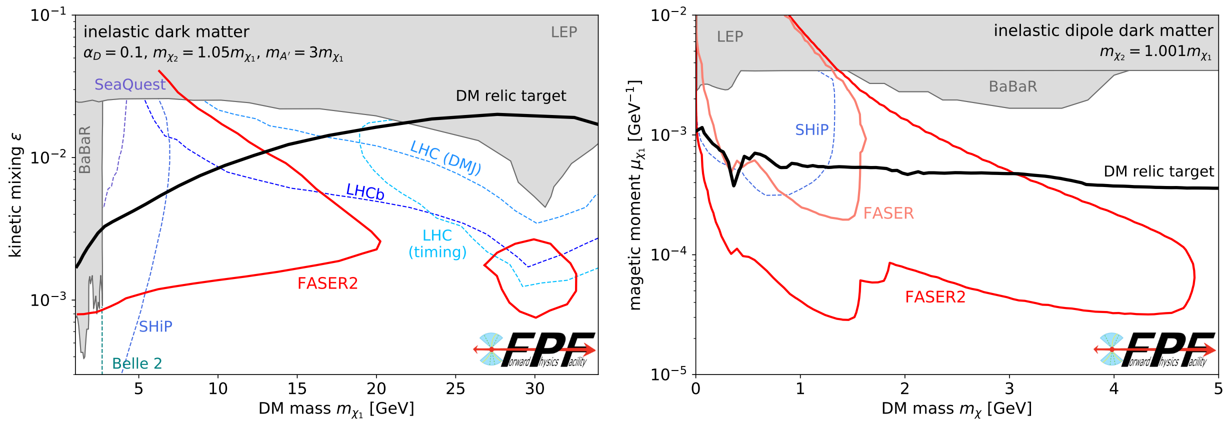

FIG. 4. **Inelastic dark matter searches at the FPF**. The discovery potential of FASER2 and other experiments for inelastic DM. Left: For heavy inelastic DM, the high energy of the LHC allows FASER2 to probe masses up to tens of GeV [14]. Right: For light inelastic DM with very small mass splittings, the large LHC energy boosts the signal to observable energies [15]. In both scenarios, the reach of FASER2 extends beyond all other experiments, including direct and indirect DM searches, LHC experiments, and beam dump experiments, such as SHiP, and covers the cosmologically-favored parameter space corresponding to the thermal relic target (solid black lines).

the forward direction of the LHC, sufficiently energetic signals can be observed the FPF, while a corresponding signal at beam dump experiments would be below the threshold of detectability. In both scenarios FASER2 will be able to decisively test a broad swath of parameter space where DM is produced in the early universe through thermal freeze-out.

DM Scattering: Another scenario of interest arises when the DM is significantly lighter than the mediator. In this case, the mediators produced in LHC proton collisions decay "invisibly" to pairs of DM particles, resulting in a significant flux of DM particles directed in the forward region at the LHC. Such DM can then be detected through its scattering with electrons and nuclei at FPF detectors, such as FLArE and FASERν2 [12, 17, 18]. In simple dark sector models with a dark photon or hadrophilic vector mediator, these experiments will be able to probe new regions of parameter space that are compatible with a thermally-produced DM relic abundance. The capability of FLArE and FASERν2 to detect the scattering of DM provides an experimental probe that is complementary to dedicated missing energy/momentum experiments and an additional window into the interactions of the DM.

B. New Particles

The many experimental signatures and broad range of BSM particle masses that can be probed at the FPF, from MeV up to the TeV scale, provide the foundation for a broad BSM physics program that will address fundamental questions in particle physics in a manner that is complementary to other existing and proposed facilities. Here we illustrate two representative examples of such unique search opportunities.

Millicharged Particles: The prospects for millicharged particle (mCP) searches at the FPF are shown in the left panel of Fig. 5. Such particles provide an interesting BSM physics target, both for their possible implications for the principle of charge quantization and as a candidate for a strongly interacting sub-component of DM. FORMOSA, a proposed scintillator-based experiment at the FPF, will have world-leading sensitivity to mCPs [13]. When compared to existing bounds and projections from several other ongoing or proposed experiments, FORMOSA benefits from the

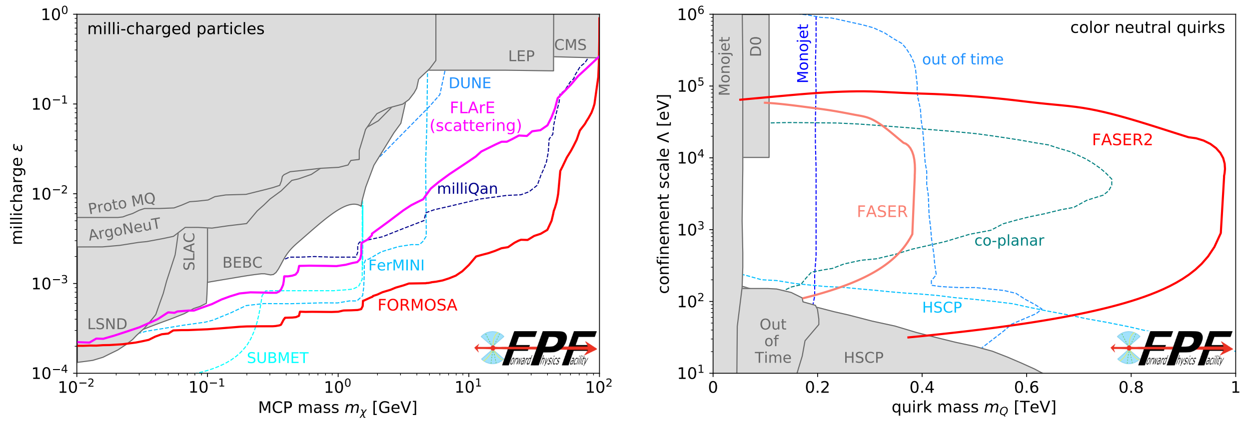

FIG. 5. **New particle searches at the FPF.** Left: The discovery reach of FORMOSA and FLArE for millicharged particles [13, 19]. Right: The discovery reach of FASER and FASER2 for color-neutral quirks [20]. In both panels, we also show existing bounds (gray shaded regions) and projected sensitivities of other experiments (dashed contours).

high-energy LHC collisions and the enhanced mCP production in the forward region, enabling the most sensitive probe of mCPs in the broad mass range from 100 MeV to 100 GeV.

Quirks: Quirks ($\mathcal{Q}$) are new particles that are charged under both the SM and an additional strongly-interacting gauge force. After they are produced at a collider, $\mathcal{Q}\bar{\mathcal{Q}}$ pairs then travel together down the beamline, bound together by a hidden color string. Discovery prospects for quirks are shown in the right panel of Fig. 5. For hidden confinement scales $\Lambda \gtrsim 100$ eV, current bounds do not even exclude quirk masses of 100 GeV. At the same time, FASER2 will probe masses up to 1 TeV, a range motivated by neutral naturalness solutions to the gauge hierarchy problem [21]. Such heavy quirks cannot be produced in fixed-target experiments and demonstrate another unique search capability of forward detectors at high-energy colliders.

C. Neutrino Physics

The LHC is the highest-energy particle collider built to date, and it is therefore also the source of the most energetic neutrinos produced in a controlled laboratory environment. Indeed, the LHC generates intense, strongly collimated, and highly energetic beams of both neutrinos and anti-neutrinos of all three flavors in the forward direction. Although this has been known since the 1980s [22], only recently have two detectors, FASERν [23] and SND@LHC [24], been installed to take advantage of this opportunity. These pathfinder experiments have just recently directly observed collider neutrinos for the first time [25–27]. By the end of LHC Run 3 in 2026, these experiments are expected to detect approximately 10^4 neutrinos. The FPF experiments, with larger detectors and higher luminosities, are projected to detect 10^5 electron neutrino, 10^6 muon neutrino, and 10^4 tau neutrino interactions, providing approximately 100 times more statistics over the current experiments, enabling precision measurements for all three flavors, and distinguishing tau neutrinos from anti-neutrinos for the first time.

Neutrino Event Rates: Fig. 6 (top) displays the expected precision of FPF measurements of the

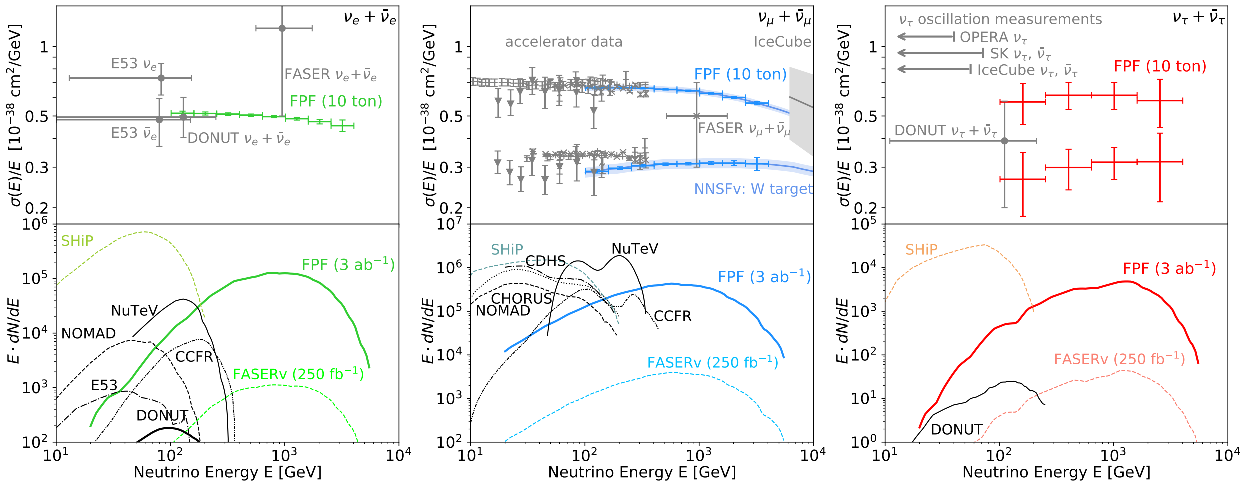

FIG. 6. **Neutrino yields and cross sections at the FPF.** The expected precision of FPF measurements of neutrino interaction cross sections (top, statistical errors only) and the spectrum of neutrinos interacting in the FPF experiments (bottom) as a function of energy for electron (left), muon (middle), and tau (right) neutrinos. Existing data from accelerator experiments [28], IceCube [29], and the recent FASERν result [30] are also shown, together with the prospects for SHiP.

neutrino-nucleon charged-current scattering cross sections for all three neutrino flavors. The low-energy region has been well-constrained by neutrino experiments using existing accelerators [28]. IceCube has also placed constraints on the muon neutrino cross section at very high energies using atmospheric neutrinos, although with relatively large uncertainties [29]. The bottom panels show the expected energy spectra of interacting neutrinos at the FPF, as estimated using EPOS-LHC [31] to simulate light hadrons and POWHEG matched with Pythia [32] to simulate charm hadron production and the fast neutrino flux simulation [33] to obtain the neutrino spectrum. The collider neutrino energy spectrum peaks at $\sim$ TeV energies, where currently no measurements exist. We also display the expected neutrino fluxes at SHiP, which peak at much lower ($\lesssim$ 100 GeV) energies.

Tau Neutrino Precision Measurements: Although only a few handfuls of tau neutrino interactions have been identified by previous experiments, thousands of tau neutrinos will be interacting in the FPF detectors. The FASERν2 detector will be able to detect them, definitively observe the anti-tau neutrino for the first time, and open up a new window to an era of tau neutrino precision studies at TeV energies. In particular, these observations will enable tests of lepton flavor universality. Deviations from universality may be parameterized, for example, by neutrino non-standard interactions (NSI) [35]. An example of FASERν2's sensitivity to probe NSIs associated with tau neutrinos is shown in Fig. 7, which utilizes the unique composition of the neutrino beam at the LHC.

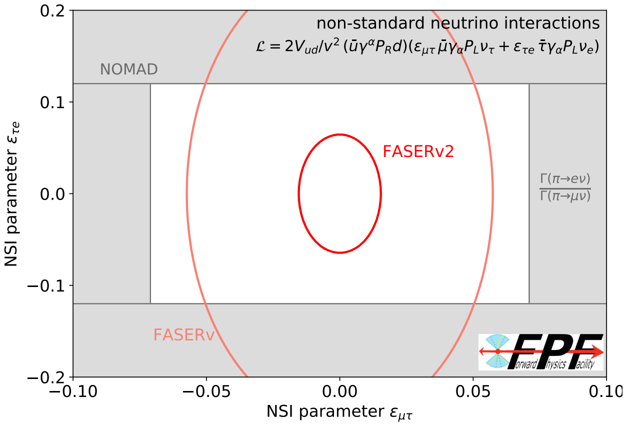

FIG. 7. **Precision tau neutrino studies at the FPF.** The projected sensitivity of FASERν2 to neutrino NSI parameters that violate lepton flavor universality [34].

Neutrino-philic New Physics: The large intensity and energy of the LHC neutrino beam at the LHC also provides a variety of novel opportunities to search for new physics. This includes searches for new neutrino-philic mediators that modify the predicted tau-neutrino flux at the FPF [18, 36]; searches for modulinos or sterile neutrinos with multi-eV masses, leading to visible oscillation patterns [9, 37, 38]; searches for anomalous electromagnetic properties of neutrinos [39]; searches for neutrino NSIs that modify neutrino production or neutrino scattering [34, 35, 40]; searches for neutrino self-interactions and neutrino-philic mediators to DM [41]; and constraints on BSM neutrino interactions through measurements of rare scattering processes, e.g., neutrino trident production [42].

D. QCD

The FPF offers unprecedented potential for innovative studies in QCD and hadronic structure. Representative targets are summarised in Fig. 8, classified into whether sensitivity arises from production at the ATLAS IP or from scattering at the FPF. Neutrino production in pp collisions constrains the gluon parton distribution function (PDF) down to $x \sim 10^{-7}$ [43, 44], charm production [45], forward hadron production [34], non-linear QCD dynamics [46, 47], and intrinsic charm [48, 49], among other phenomena. In turn, neutrino scattering at the FPF enable map-

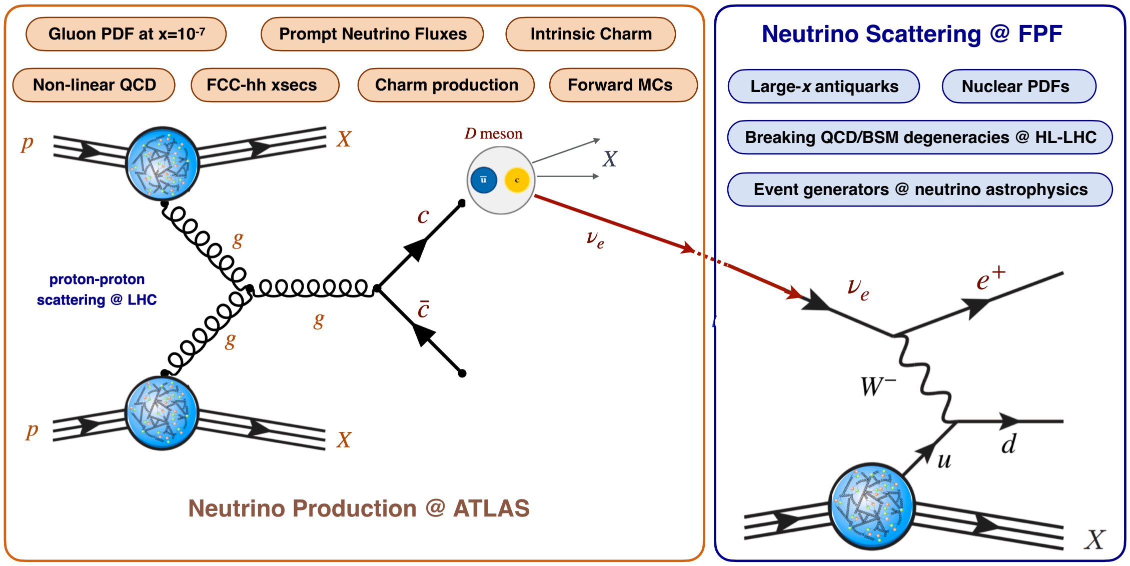

FIG. 8. **QCD physics at the FPF.** Representative QCD targets at the FPF, classified into production at the ATLAS IP and scattering at the FPF neutrino detectors.

ping large-x nucleon structure [50], breaking degeneracies between BSM signals and QCD effects in high-p_T tails at the HL-LHC [51, 52], and tuning generators for neutrino astrophysics [53–56].

FPF Neutrino Measurements Enhance HL-LHC Discovery Prospects: Dedicated projections for neutrino DIS at the FPF [50] demonstrate that the expected $\mathcal{O}(10^5)$ electron-neutrino and $\mathcal{O}(10^6)$ muon-neutrino interactions provide stringent constraints on the proton PDFs. These neutrino collisions cover an (x, Q^2) range that overlaps with that of the Electron-Ion Collider (EIC) [57], while probing complementary flavour combinations. D-meson tagging capabilities in

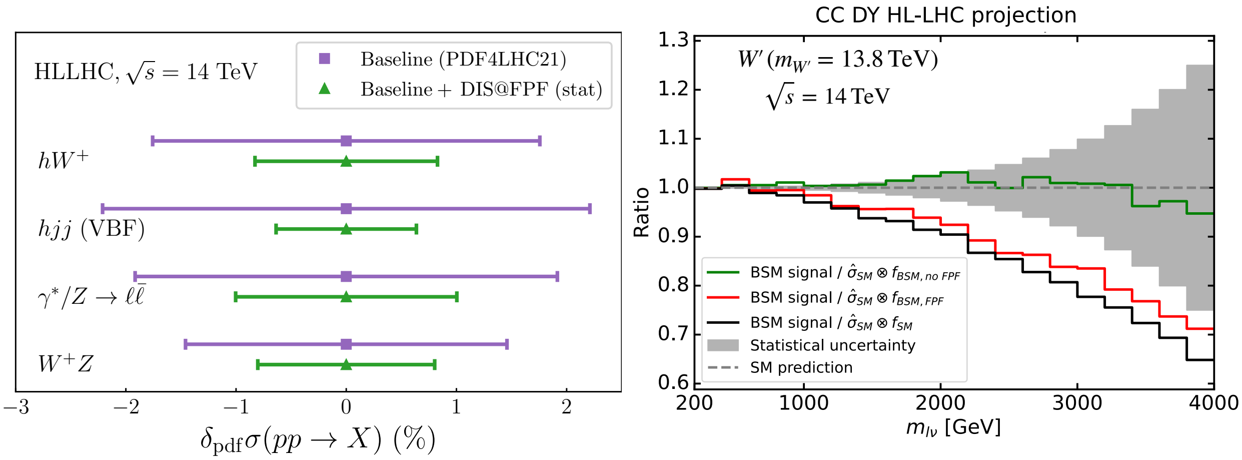

FIG. 9. **Impact of FPF neutrino measurements on traditional BSM Searches at the HL-LHC.** Left: Reduction of uncertainties on Higgs- and weak gauge-boson cross sections at the HL-LHC, enabled by neutrino DIS measurements at the FPF. Right: Evidence for a new heavy W' boson with $m_{W'} = 13.8$ TeV would be reabsorbed in a PDF fit including Drell-Yan data from the HL-LHC ($f_{\rm BSM,noFPF}$), unless the PDFs are constrained by "low energy" FPF neutrino data ($f_{\rm BSM,FPF}$).

the FPF neutrino experiments enable disentangling quark and antiquark flavours. The impact of DIS neutrino measurements at the FPF on the traditional HL-LHC program is twofold. On the one hand, FPF-constrained PDFs enable more precise theoretical predictions for core processes at the HL-LHC such as Higgs, Drell-Yan, and diboson production (left panel of Fig. 9). Measurements of these cross sections at ATLAS and CMS are therefore more sensitive to BSM physics. On the other hand, if BSM signals are present in high-p_T tails at the HL-LHC, they could inadvertently be reabsorbed into a PDF fit [51, 52]. Breaking this degeneracy between QCD and BSM effects in high-energy scattering is possible by including the "low-energy" FPF data into the PDF fit. For instance, as demonstrated in the right panel of Fig. 9, evidence for a new heavy W' boson with mass $m_{W'} = 13.8$ TeV would be reabsorbed in a PDF fit including Drell-Yan data from the HL-LHC ($f_{\mathrm{BSM,noFPF}}$) unless the PDFs are constrained with the FPF neutrino data ($f_{\mathrm{BSM,FPF}}$). FPF data therefore greatly enhances the discovery potential of ATLAS and CMS for high mass particles. Neutrino DIS at the FPF also opens a novel window on the 40-year-old conundrum of whether intrinsic charm (or even bottom) quarks exist in the proton [48, 49, 58].

Small-x QCD from Charm Production: The LHC neutrino fluxes depend sensitively on the mechanisms for forward light and heavy hadron production in pp collisions [32, 33]. The overall normalization of the muon-neutrino flux can be measured at the per-mille level at the FPF [50]. Measurements of forward D-meson production at LHCb can constrain the gluon PDF down to $x \sim 10^{-5}$ [43, 45]. By defining tailored observables where theory uncertainties cancel out, such as the ratio between electron and tau neutrino event rates, FPF measurements can be used to pin down the gluon PDF down to $x \sim 10^{-7}$ [44], as shown in Fig. 10. Such measurements inform the study of novel QCD dynamics at small-x, a region where non-linear and BFKL-like effects are expected to dominate, as highlighted by the DGHP24 predictions [46] for the gluon PDF based on saturation (recombination) effects built into the DGLAP evolution. Constraints on the small-x gluon PDF would be instrumental to inform FCC-hh cross sections, since at $\sqrt{s} = 100$ TeV even Higgs and gauge boson production becomes a "small-x" process with potentially large corrections from BFKL resummation [59, 60]. These constraints on small-x QCD are also relevant for astroparticle physics.

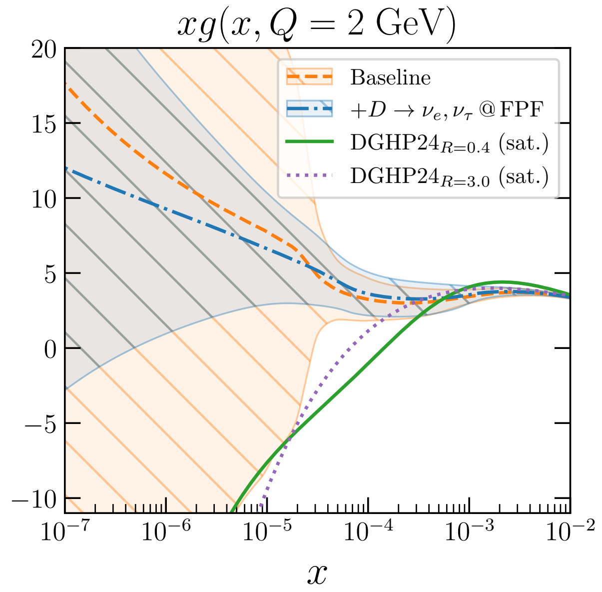

FIG. 10. **Small-x QCD at the FPF.** Impact of FPF data on the small-x gluon PDF, compared with non-linear QCD (saturation) models.

Neutrino Event Generators: The robust interpretation of FPF measurements demands state-of-the-art Monte Carlo event generators for neutrino scattering at TeV energies. Such generators, based on higher-order QCD corrections and matched to modern parton showers, are also relevant to model high-energy neutrino scattering at neutrino telescopes such as IceCube [61] and KM3NeT [62]. Testing and validating neutrino event generators, such as the POWHEG-based ones presented in Refs. [53, 55, 56], on FPF data is also instrumental for the FPF BSM program, with neutrino signals representing the leading background in many searches. Measurements of fragmentation functions in neutrino DIS also probe the cold nuclear medium of the target nucleus, complementing eA scattering analyses at the EIC.

E. Astroparticle Physics

Besides addressing key questions in astrophysics, high-energy cosmic-ray and neutrino experiments provide unique access to particle physics at center-of-mass energies that are an order of magnitude higher than LHC *pp* collisions [63, 64]. The FPF provides unique opportunities for interdisciplinary studies at the intersection of particle and astroparticle physics [10, 65–67].

The Muon Puzzle: For many years, the experimental measurements of the number of muons in high- and ultra-high-energy cosmic-ray air showers have appeared to be in tension with model predictions [68–73]. This conundrum has been dubbed the cosmic-ray muon puzzle. Various air-shower models [31, 74–79] can be tested under controlled experimental conditions at the FPF, because the ratio of the low-energy electron and muon neutrino fluxes is a proxy for the charged kaon to pion production rate. The differences in the predicted fluxes exceed a factor of two, which is much larger than the expected statistical uncertainties at the FPF [33]. Since the muon puzzle is assumed to be of soft-QCD origin [64], there is also a strong connection to the QCD program of the FPF and dedicated QCD measurements will further help to understand particle production in cosmic-ray air showers. Thorough analyses have suggested that an enhanced rate of strangeness production in the forward direction could explain the observed discrepancies [64, 80–82]. A specific example accounting for enhanced strangeness production is the simple phenomenological (one-parameter) `piKswap` model which predicts a significant increase of electron neutrinos with energies below 1 TeV [83, 84] that can be tested at the FPF. The blue curve in Fig. 11 illustrates the projected sensitivity of the FPF to the `piKswap` model.

Atmospheric Neutrino Fluxes: High-energy neutrinos of astrophysical origin are routinely observed by large-scale neutrino telescopes, such as IceCube [61] and KM3NeT [62], and atmospheric neutrinos produced in extensive air showers are an irreducible background for these searches. Neu-

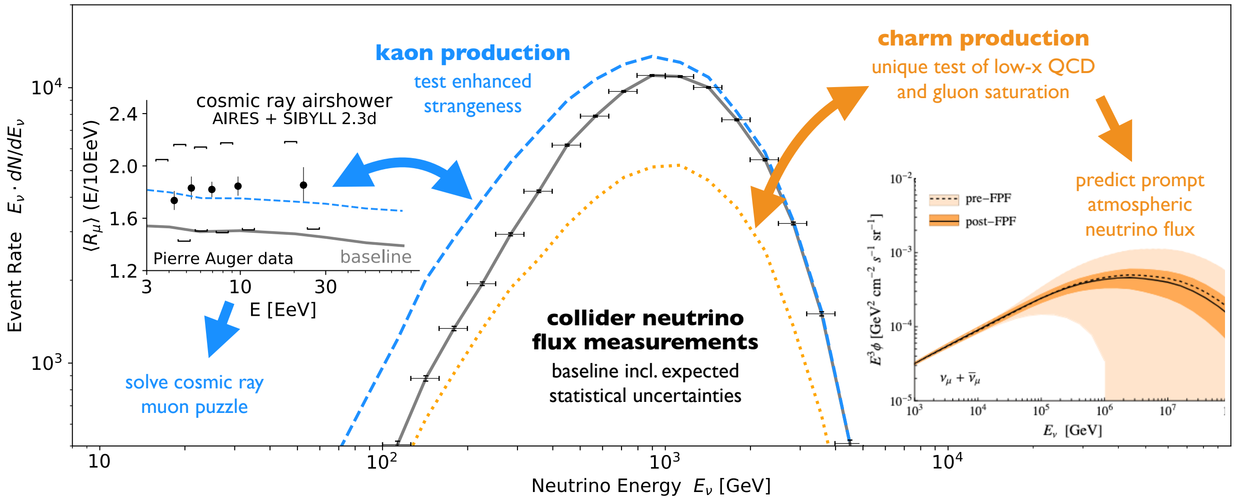

FIG. 11. **Astroparticle physics at the FPF.** Expected energy spectrum of interacting electron neutrinos in FLArE, including statistical uncertainties (solid gray band). The colored dashed contours illustrate two examples of physics that can change the expected flux and be probed at the FPF: enhanced kaon production that solves the muon puzzle, and gluon saturation at small-x. Left: Dimensionless muon shower content R_μ as predicted by the `piKswap` model through simulations with `AIRES + SIBYLL 2.3` [74, 85] compared with data from the Pierre Auger Observatory [68]; for details, see [83]. Right: Reduction of PDF uncertainties on the prompt neutrino flux Φ enabled by FPF data as a function of E_ν; see also Fig. 10.

trinos at high energies above 1 TeV are mainly produced in charm hadron decays. The production of charm quarks is dominated by gluon fusion and can be described using perturbative QCD [86]. Measurements of the neutrino flux at the FPF therefore provide access to both the very high-x and the very low-x regions of the colliding protons. These measurements yield information about high-x PDFs, in particular intrinsic charm, as well as novel QCD production mechanisms, such as BFKL effects and non-linear dynamics, well beyond the coverage of other experiments and providing key inputs for astroparticle physics. One specific example of novel QCD dynamics that may affect the prompt neutrino fluxes is gluon saturation, which causes a suppression of the gluon density at low-x; see Fig. 10. This mechanism leads to a reduced flux of TeV-energy neutrinos at the FPF, as illustrated by the orange curve in Fig. 11. Therefore, FPF measurements will provide stringent constraints on the prompt atmospheric neutrino flux, contributing to the scientific program of large-scale neutrino telescopes. This is further quantified in Fig. 11, showing theoretical predictions for the prompt muon-neutrino flux based on the formalism of Refs. [87, 88], considering only PDF uncertainties, before and after FPF constraints are included. Although other sources of theory uncertainty contribute to the total error budget, Fig. 11 demonstrates the strong sensitivity of the FPF to the mechanisms governing atmospheric neutrino production from charm decays.

II. THE FACILITY

The FPF facility has been studied by CERN experts over the last four years, with technical studies detailed in Refs. [89–91]. The work has benefited from the vast experience at CERN in designing and implementing many similar large underground facilities, particularly the recent HL-LHC underground works at the ATLAS and CMS IPs. Many of the same technical solutions can be adopted for the FPF, and lessons learnt can also be applied.

Site Selection and Cavern Design: A site optimization to find the best location for the FPF facility was carried out. This identified an optimal site 627 m west of the ATLAS IP (IP1), on CERN land in France, as shown in Fig. 12. Following this, the facility design has been through several iterations to optimize the layout for the proposed detectors, along with the needed technical infrastructure. The current baseline design is shown in Fig. 13. This includes a 75 m-long, 12 m-wide underground cavern, with a dedicated experimental area (65 m long) and a service cavern (5 m long), as well as an 88 m-deep shaft and the associated surface building for access and services. The closest point between the underground cavern and the LHC tunnel is 10 m, as required by the civil engineering and radiation protection teams.

Site Investigation and Geological Conditions: In Spring 2023, a site investigation study was carried out where a 20 cm-diameter, 100 m-deep core was drilled at the proposed location of the FPF shaft. Analysis of the extracted core confirmed that the geology is good for the planned excavation works, and no show stoppers were identified. A Class 4 costing for the civil engineering work has been carried out, based on similar work carried out at CERN in the last decade and taking into account the findings of the site investigation. The costing methodology has been cross checked by an external civil engineering consultant. The cost estimate is 35 MCHF for the underground works, shaft, and surface buildings. A detailed breakdown of these costs is given in Appendix A. The expected time for the civil engineering works is 3 years.

Excavation Work and Vibrations: The possibility of carrying out the FPF excavation work during beam operation will allow much more flexibility in the FPF implementation schedule. However, concerns have been raised that the excavation works could impact beam operations of the LHC or SPS, leading to beam losses and possible beam dumps. The CERN accelerator group has

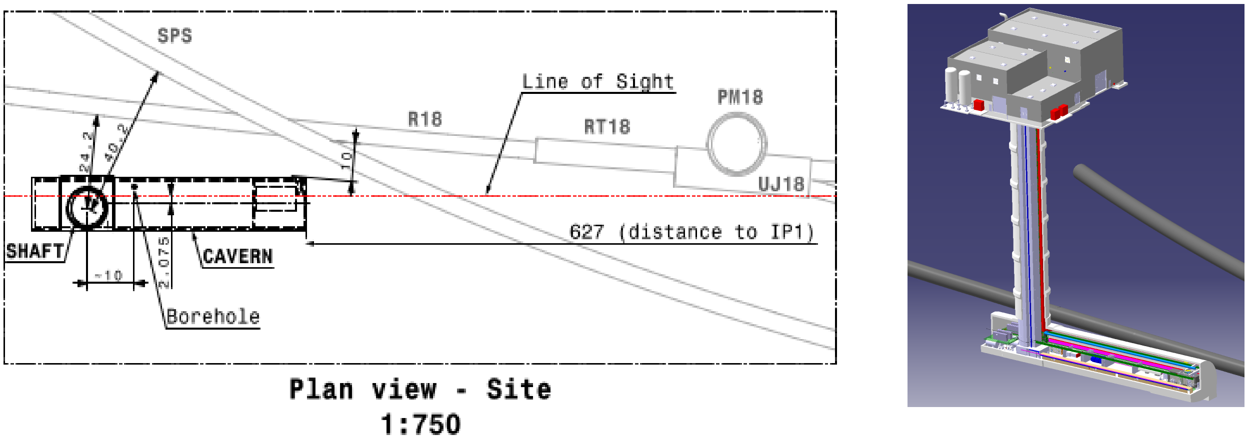

FIG. 12. Left: Plan view showing the FPF location. Right: 3D view of the Facility.

carried out detailed studies of the effect of the expected vibration level from the excavation on beam operation performance, as documented in Ref. [91]. The conclusion of these studies is that no problems are foreseen, and the excavation can be carried out during beam operations.

Muon Fluxes: The expected muon background rate in the FPF has been estimated using FLUKA [92] simulations. These simulations include a detailed description of the infrastructure between IP1 and the FPF. For the LHC Run 3 setup, the simulations have been validated at the $\mathcal{O}(25\%)$ level with FASER [93] and SND@LHC [94] data. However, for the HL-LHC, much of the accelerator infrastructure (magnets, absorbers, etc.) in the relevant region will change. As shown in Fig. 14, for the baseline HL-LHC luminosity of 5×10^{34} cm^{-2} s^{-1}, FLUKA simulations predict a muon flux of 0.6 cm^{-2} s^{-1} within 50 cm of the LOS, with the flux substantially higher when going to 2 m from the LOS in the horizontal plane. In general, the expected muon rate is acceptable for the proposed experiments, however reducing the rate would be beneficial. Here, studies on the effectiveness of installing a sweeper magnet in the LHC tunnel or using the beam corrector magnets to reduce the flux are ongoing.

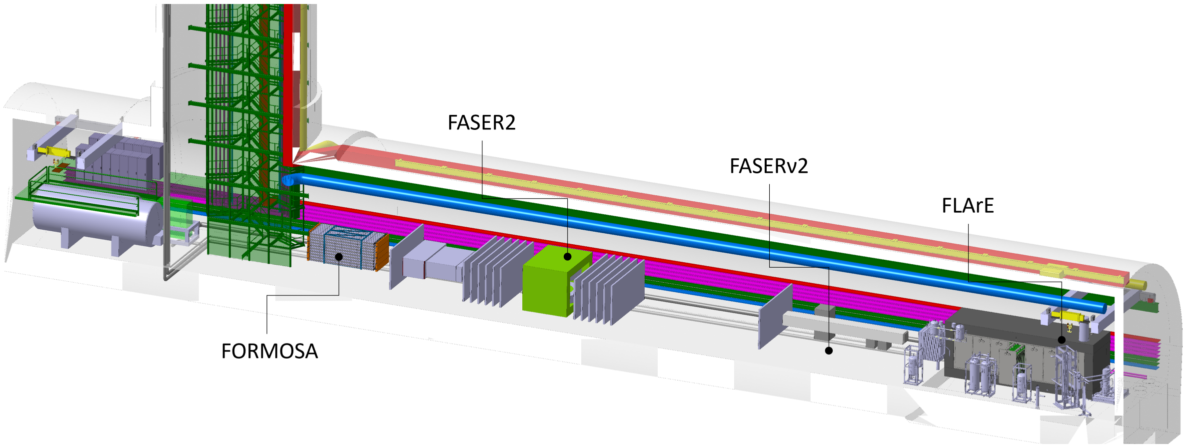

FIG. 13. The baseline layout of the FPF facility, showing the four proposed experiments and the large infrastructure.

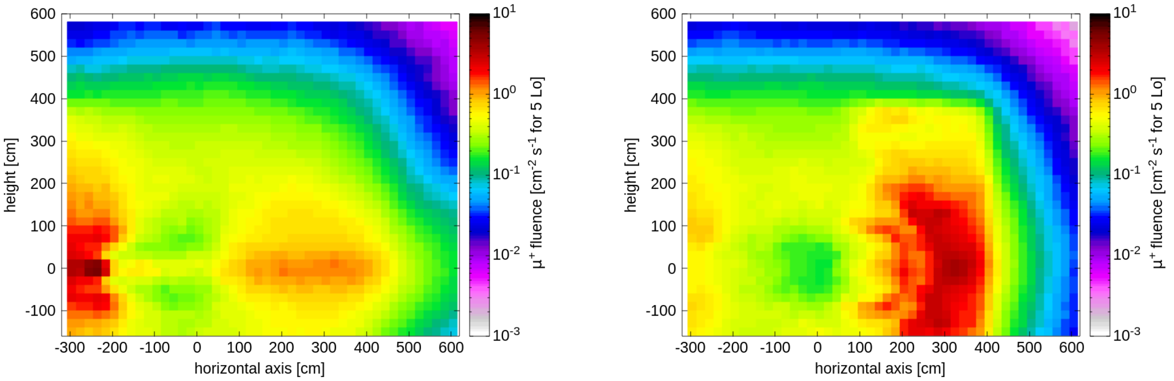

FIG. 14. The muon fluence rate for μ^- (left) and μ^+ (right) in the transverse plane in the FPF cavern for the HL-LHC baseline luminosity of 5×10^{34} cm^{-2} s^{-1}. The coordinate system is defined such that $(0, 0)$ is the LOS.

Radiation Levels and Safety: FLUKA simulations have also been used to assess the radiation level relevant for the detectors, which is estimated assuming the HL-LHC baseline integrated luminosity of 360 fb^{-1} per year. The neutron field that can cause radiation-induced damage to silicon detectors has been assessed to be less than 10^7 cm^{-2} y^{-1} Silicon 1 MeV neutron equivalent fluence (many orders of magnitude lower than that in the LHC experiments). The annual high-energy hadron equivalent fluence, determining the single event error rate in electronics, does not exceed 3×10^6 cm^{-2} y^{-1}, which is the threshold adopted in the LHC for declaring an area safe from the radiation to electronics (R2E) point of view [95].

Being able to access the cavern during beam operations will be extremely valuable for detector installation, commissioning, and maintenance tasks. It will also allow the experiments to be upgraded or even replaced, as may be necessary to respond to the evolution of the physics landscape over the time period of the HL-LHC. FLUKA simulations have been used to assess the radiation level in the FPF cavern during beam operation. These studies show that the radiation source will be solely from muon-induced particles. The expected radiation level will be low enough for people to access the cavern during beam operation, provided they are trained as radiation workers, carry a dosimeter, and are there for less than 20% of the time integrated over a year. However, some parts of the cavern may be classified as local short stay areas.

Transport and Detector Integration: Integration studies have shown that the proposed experiments (in their current form) can be installed and fit into the baseline cavern, including their main associated infrastructure. Standard infrastructure and services that have been considered so far include cranes and handling infrastructure, electrical power, ventilation systems, fire/smoke safety, access, and evacuation systems. A very preliminary costing of these services (based on existing CERN standard solutions) is at the level of less than 10 MCHF, giving a total costing of the facility, including both civil engineering and outfitting, of around 45 MCHF.

III. FASER2

FASER2 is a large-volume detector comprised of a spectrometer, electromagnetic and hadronic calorimeters, veto detectors and a muon detector, that is designed for sensitivity to a wide variety of models of BSM physics and for precise electron and muon reconstruction for neutrino measurements. It builds on positive experience gained from the successful operation of the existing FASER

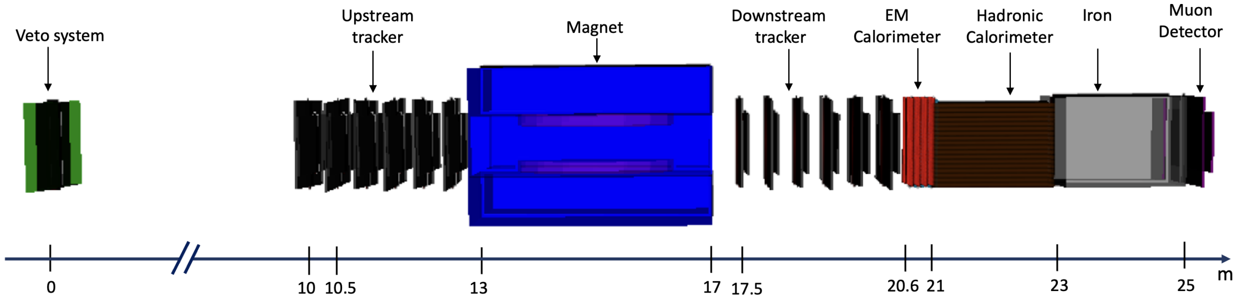

FIG. 15. Visualisation of the full FASER2 detector, showing the veto system, uninstrumented 10 m decay volume, tracker, magnet, electromagnetic calorimeter, hadronic calorimeter, iron absorber and muon detector.

experiment [96], a much smaller detector, which was constrained to be situated within an LHC transfer tunnel. The FASER2 detector, specifically designed for the FPF facility, is much larger (by a factor of ~ 600 in decay volume size) and includes new detector elements. It provides an increase in reach for various BSM signals of several orders of magnitude compared to FASER and allows sensitivity to models that were previously out of reach, such as dark Higgs, heavy neutral lepton, and axion-like particle models, as studied in Refs. [11, 23, 97]. There is particularly unique sensitivity in inelastic dark matter and in searches for quirks in a mass range motivated by naturalness arguments, as discussed in Sec. I.

In addition to the BSM case for FASER2, the SM neutrino program at the FPF will rely on the identification of muons (and potentially electrons) from neutrino decays and precise measurement of their momentum and charge. The FASER2 spectrometer will be integral for these measurements for both FASERν2 and FLArE.

Figure 15 shows a rendering of the GEANT4 model of the full FASER2 detector. This design is the result of several iterations and improvements, but it is still a work in progress. The overall layout is largely driven by the spectrometer, which is itself constrained by considerations relating to deliverable and affordable magnet technology. This leads to a baseline detector configuration consisting of a split spectrometer with a large-volume dipole magnet. The magnet has a rectangular aperture of 1 m in height and 3 m in width. This also defines the transverse size of the decay volume, which is the 10 m uninstrumented region upstream of the first tracking station (a $2.6 \times 1 \times 10$ m^3 cuboid) and downstream of the first veto station. Maximising the transverse size is a general design requirement driven by the need to have sufficient acceptance for BSM particles originating from heavy flavour decays and charged leptons arising from neutrino interactions in FLArE. Studies are ongoing as to whether the decay volume would need to be under vacuum or filled with low-density gas, i.e., helium, to achieve background-free measurements. A more square (e.g., 1.7×1.7 m^2) aperture is also under consideration, as it improves the acceptance of muons from FLArE by 5-10% without a significant degradation in LLP sensitivity.

The baseline integrated magnetic field strength is 2 Tm. This is optimised based on simulations that demonstrate that the required charged particle separation, momentum resolution, and charge identification are obtained for the BSM and neutrino programme, while keeping the field strength to an acceptable minimum to reduce cost. Superconducting magnet technology is required to maintain such a field strength across a large aperture. Recent investigations by KEK magnet experts, along with discussions with manufacturing experts at Toshiba in Japan and Tesla Engineering in the UK, have demonstrated that this design is feasible at an acceptable cost (~ 4 MCHF) and lead-time (3.5 years). Alternative backup options are also being investigated to make use of industrial magnets with a smaller aperture (circular with 1.6 m diameter) and lower field strength (~ 1.5 Tm). These magnets are commercially available at a lower cost, and while they do lead to a limited degradation in sensitivity, this is not significant enough to put the main physics goals out of reach.

For most FASER2 sub-detectors, a performant baseline is achievable from simpler well-understood detector technologies that will allow the major physics goals to be achieved. However, more advanced technologies are also under consideration to augment these baseline capabilities, and the evaluation of these has undergone the most scrutiny so far due to the higher associated cost. Such augmentations are especially appealing in the case that they can come via existing R&D activities, for example, in the context of future colliders, where FASER2 can act as a mid-term testbed.

The tracking detectors are foreseen to use a SiPM and scintillating fiber tracker technology, based on LHCb's SciFi detector [98]. This technology gives sufficient spacial resolution ($\sim 100\ \mu$m) at a significantly reduced cost compared to silicon detectors. The use of silicon-based tracking detectors will be explored for the interface between FASER2 and FASERν2, and for the first tracking station downstream of the decay volume. Possible augmentation utilising the LHCb MightyPix technology [99] is under investigation for potential improvement in particle separation power in both the first tracker layer and in the central region of the transverse plane, where the LLP energy is higher and decay products more collimated.

A simple lead-scintillator calorimeter would be sufficient for the reconstruction of energy deposits from electrons and hadronic decay products of LLPs. A more advanced calorimeter is also under study to be based on dual-readout calorimetry [100, 101] technology, especially for the central region. This builds upon experience of existing prototypes for future collider R&D, but modified for the specific physics needs of FASER2: spatial resolution sufficient to identify particles at $\sim 1-10$ mm separation; good energy resolution; improved longitudinal segmentation with respect to FASER; and the capability to perform particle identification, separating, for example, electrons and pions.

The ability to identify separately electrons and muons would be very important for signal characterization, background suppression, and for the interface with FASERν2. To achieve this, $\mathcal{O}(10)$ interaction lengths of iron will be placed after the calorimeter, with sufficient depth to absorb pions and other hadrons, followed by a detector for muon identification, for which additional SciFi planes could be used. Finally, the veto system will be required to reject muon rates of approximately 20 kHz. Scintillator-based approaches have proven to be sufficient for this in FASER, and a similar, but re-optimised, design is foreseen for FASER2. The event rate and size are much lower than most LHC experiments, so the trigger needs are not expected to be a limiting issue. For instance, it is expected that it will be possible to significantly simplify the readout of the tracker, with respect to what is used in the LHCb SciFi detector.

Various performance studies have been performed to assess different design considerations and technologies for FASER2. Metrics such as momentum resolution, LLP sensitivity, and geometrical acceptance have been studied both in terms of physics performance and the implied detector technology complexity and cost. Different simulation tools have been utilised for these studies: the FORESEE [102] package is used for the simulation and event generation of LLP production from forward hadrons; the Geant4 [103] simulation framework is used for the propagation of particles through a magnetic field in the LLP decay product separation studied; and the ACTS [104] tool is used for track reconstruction studies.

An illustration of such studies is provided in the following for the expected momentum resolution. For the baseline detector outlined above, with an intrinsic resolution of 100 μm and 2 Tm integrated field strength, a muon momentum resolution of approximately 2(4)% is achieved for 1(5) TeV muons. This is expected to be sufficient for the physics goals of FASER2. Studies show the baseline design to be quite robust: this performance is stable under a range of magnetic field strengths, and appreciable degradation only appears with a significantly worse intrinsic resolution. The momentum resolution was also studied as a function of the amount of material in each tracker layer and only when approaching an interaction length is a significant loss in resolution observed. Studies were also performed to understand the possible impact of detector misalignnment. This shows that significant misalignments can be corrected using a track-based alignment method, with a precision of $\sim 50\ \mu$m obtainable.

The FASER2 experiment will be essential to maximise the physics potential of the FPF. The baseline detector design has been optimised to obtain the required physics performance in an affordable way, but several systems could be upgraded to improve the performance at higher cost. Given the importance of the FASER2 magnet in the design, significant work has been carried out to find a baseline solution for this, with an alternative option using commercially-available magnet units also being considered.

IV. FASERν2

FASERν2 is a 20-ton neutrino detector located on the LOS, a much larger successor to the FASERν [105] detector in the FASER experiment. With the FASERν detector, the first evidence for neutrino interaction candidates produced at the LHC was reported in 2021 [106], and the first measurements of the ν_e and ν_μ interaction cross sections at TeV energies were reported in 2024 [30]. These results confirms the FASERν emulsion detector's ability to deliver physics measurements in the LHC environment.

An emulsion-based detector will identify heavy flavor particles produced in neutrino interactions, including tau leptons and charm and beauty particles. FASERν2 can perform precision tau neutrino measurements and heavy flavor physics studies, testing lepton universality in neutrino scattering and new physics effects, as well as providing important input to QCD and astroparticle physics, as described in Sec. I.

The left panel of Fig. 16 shows a schematic of the proposed FASERν2 detector, which is composed of 3300 emulsion layers interleaved with 2-mm-thick tungsten plates. The total volume of the tungsten target is 40 cm × 40 cm × 6.6 m, with a mass of 20 tons. The emulsion detector will

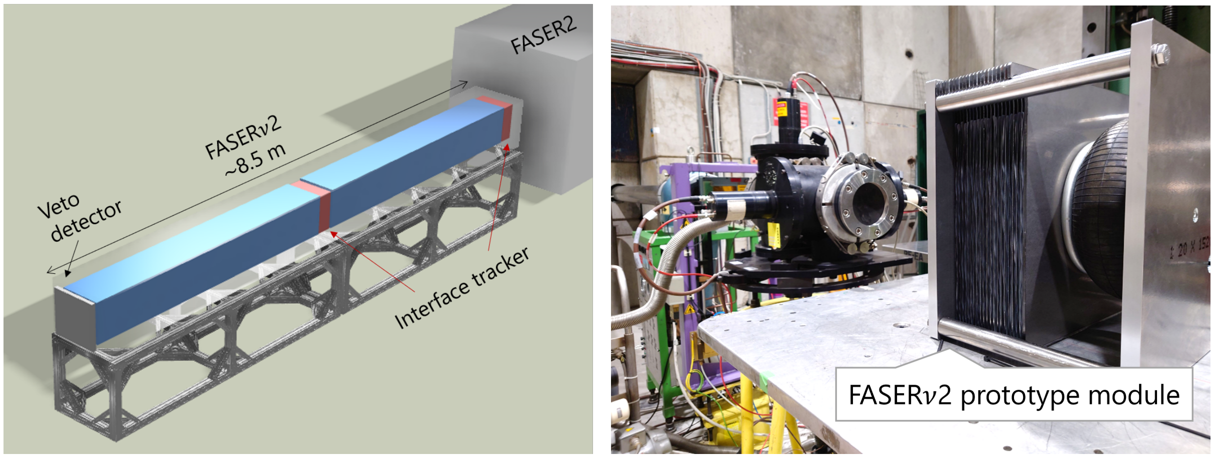

FIG. 16. Left: Design of the FASERν2 detector. Right: FASERν2 prototype module on the SPS-H8 beamline.

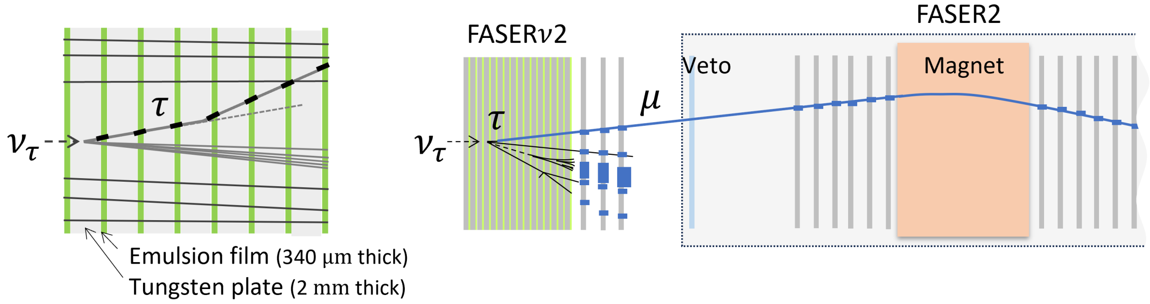

FIG. 17. Left: Tau decay topology in the emulsion detector. Right: Charge measurement for a muon from a tau decay.

be placed in a cooling box and kept at around 10°C to avoid fading of the recorded signal. The detector will be placed directly in front of the FASER2 spectrometer along the LOS. The FASERν2 detector will also include a veto system and interface detectors to the FASER2 spectrometer, with one interface detector in the middle of the emulsion modules and the other detector downstream of the emulsion modules. These additional systems will enable a FASER2-FASERν2 global analysis and make measurement of the muon charge possible, a prerequisite for $\nu_\tau/\bar{\nu}_\tau$ separation. The veto system will be scintillator-based, and the interface detectors could be based on silicon strip sensors or scintillating fiber tracker technology. The detector length, including the emulsion films and interface detectors, will be approximately 8.5 m.

A mechanical prototype has been produced to test critical technical challenges, namely applying pressure to fix sub-micrometer alignment and assembly under room light in the FPF experimental hall. As shown in the right panel of Fig. 16, a test beam experiment was performed in July 2024 at the SPS-H8 beamline, confirming the concept of the techniques. In addition to the test of a mechanical prototype, other test samples were produced and exposed to the beam. With these, one can check the long-term performance of emulsion films to take data through a year without replacing emulsion films. One can also test a new type of photo-development solution, which increases the gain of chemical amplification, which can help maximize the readout speed of the emulsion detector. The analysis of the samples is ongoing.

As the $c\tau$ of the tau lepton is 87 μm, a high-precision emulsion detector [107] is essential to detect tau decays topologically. After optimizations of the detector performance in terms of precision, sensitivity, and long-term stability, emulsion gel with silver bromide crystals of 200 nm diameter will be used, which provides an intrinsic position resolution of 50 nm. The left panel of Fig. 17 shows a tau decay topology in the emulsion detector. As shown in the right panel of Fig. 17, a global analysis that links information from FASERν2 with the FASER2 spectrometer enables charge measurements of muons from tau decays, and thereby the detection of $\bar{\nu}_\tau$ for the first time.

Emulsion detector analysis will be limited by the accumulated track density and become difficult above 10^6 tracks/cm^2 with the current tracking algorithms. New tracking algorithms will be developed to tolerate the high track density, such as with a machine learning method. To keep the accumulated track density at an analyzable level, the emulsion films will be replaced once per year. The implementation of an effective sweeper magnet to reduce the muon fluence in the FPF would be beneficial, and studies on possible designs for this are ongoing.

The emulsion film production and its readout will be conducted at facilities in Japan. The capacity of the film production facility [108] is 1200 m^2 per year. The HTS scanning system can read out ∼0.5 m^2 per hour, or 1,000 m^2 per year. Recently, an upgraded HTS system, HTS2, became operational with about two times faster speed. Scanning FASERν films with HTS2 is under testing. Analysis methodologies dedicated to TeV neutrinos are currently being developed and tested in FASERν. These methods include momentum measurements using multiple Coulomb scattering information, electromagnetic shower reconstruction, and machine learning algorithms for neutrino energy reconstruction.

FASERν2 has a clear and broad physics target, and the detector is based on a well-tested technology for tau neutrino and short-lived particle detection. Further studies are being carried out to optimize the detector performance, the detector operational environment, and the installation scheme.

V. FORMOSA

The FPF provides an ideal location for a next-generation experiment to search for BSM particles that have an electrical charge that is a small fraction of that of the electron. Although the value of this fraction can vary over several orders of magnitude, we generically refer to these new states as "millicharged" particles (mCPs). Since these new fermions are typically not charged under QCD, and because their electromagnetic interactions are suppressed by a factor of $(Q/e)^2$, they are "feebly" interacting and naturally arise in many BSM scenarios that invoke dark or otherwise hidden sectors. For the same reason, experimental observation of mCPs requires a dedicated detector.

As proposed in Ref. [13], FORMOSA will be a milliQan-type detector [109, 110] designed to search for mCPs at the FPF. FORMOSA will be technically similar to what the milliQan Collaboration has installed in the PX56 drainage gallery near the CMS IP at LHC Point 5 for Run 3 [111], but with a significantly larger active area and a more optimal location with respect to the expected mCP flux. As discussed in Sec. I and shown in Fig. 5 (left), FORMOSA has the potential to significantly extend the search for mCPs over the broad range of masses from 10 MeV to 100 GeV.

To be sensitive to the small dE/dx of a particle with $Q \lesssim 0.1e$, an mCP detector must contain a sufficient amount of sensitive material in the longitudinal direction pointing to the IP. As in Ref. [109], plastic scintillator is chosen as the detection medium with the best combination of photon yield per unit length, response time, and cost. Consequently, FORMOSA is planned to be a 1 m × 1 m × 5 m array of suitable plastic scintillator (e.g., Eljen EJ-200 [112] or Saint-Gobain BC-408 [113]). The array will be oriented such that the long axis points at the ATLAS IP and will be located on the LOS. The array contains four longitudinal "layers" arranged to facilitate a 4-fold coincident signal for feebly-interacting particles originating from the ATLAS IP. Each layer in turn contains 400 5 cm × 5 cm × 100 cm scintillator "bars" in a 20 × 20 array. To maximize sensitivity to the smallest charges, each scintillator bar is coupled to a high-gain photomultiplier tube (PMT) capable of efficiently reconstructing the waveform produced by a single photoelectron (PE). To reduce random backgrounds, mCP signal candidates will be required to have a quadruple coincidence of hits with $\overline{N}_{\mathrm{PE}} \geq 1$ within a 20 ns time window. The PMTs must therefore measure the timing of the scintillator photon pulse with a resolution of ≤ 5 ns. The bars will be held in place by a steel frame. A conceptual design of the FORMOSA detector is shown in Fig. 18 (left).

Although omitted for clarity in Fig. 18, additional thin scintillator "panels" placed on each side of the detector will be used to actively veto cosmic muon shower and beam halo particles. Finally, the front and back of the detector will be comprised of segmented veto panels using perpendicular scintillator bars. This will provide efficient identification and tracking of the muons resulting from LHC proton collisions through the detector. During Run 2 of the LHC, a similar experimental

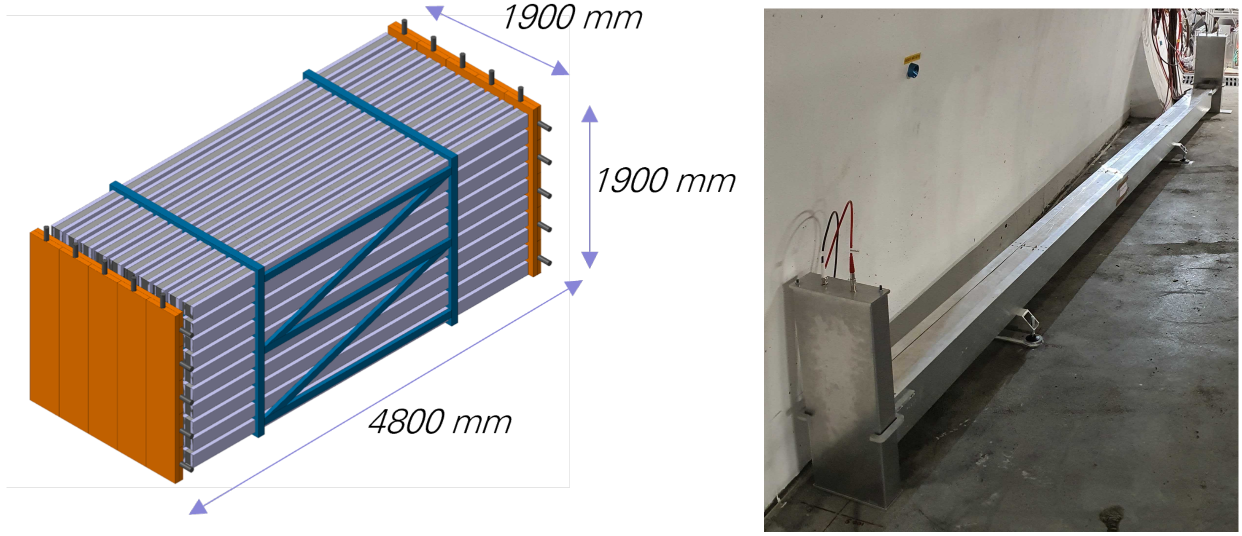

FIG. 18. Left: An engineering drawing of the FORMOSA detector. Right: The FORMOSA demonstrator taking data in the forward region of the LHC.

apparatus (the milliQan "demonstrator") was deployed in the PX56 draining gallery at LHC P5 near the CMS IP. This device was used successfully to search for mCPs, proving the feasibility of such a detector [114].

Even though the pointing, 4-layered design will be very effective at reducing background processes, small residual contributions from sources of background that mimic the signal-like quadruple coincidence signature are expected. These include overlapping dark rate pulses, cosmic muon shower particles, and beam muon afterpulses. In Ref. [111], data from the milliQan prototype was used to predict backgrounds from dark rate pulses and cosmic muon shower particles for a closely related detector design and location. Based on these studies, such backgrounds are expected to be negligible for FORMOSA. Backgrounds from muon afterpulses are considered in Ref. [13] and can be rejected by vetoing a 10 μs time window in the detector following through-going beam muons. This veto will be improved by the muon tracking provided by the segmented bars at the front and back of the detector. The feasibility of this has been shown through the operation of the FORMOSA demonstrator during Run 3 of the LHC. This is shown in Fig. 18 (right).

The FORMOSA detector is proposed to be constructed of plastic scintillator, however, in the coming years, the exciting possibility of using alternative scintillator material with significantly higher light-yield will be studied. One such material is CeBr3 scintillator (available from Berkeley Nucleonics). This provides a light yield approximately factor 30 times higher than the same length of plastic scintillator with excellent timing resolution. This would allow much lower charges to be probed with the FORMOSA detector. Further updates to the detector design are also currently being studied with the FORMOSA demonstrator in the forward region of the LHC.

VI. FLARE

FLArE is a modularized, liquid argon, time-projection chamber (TPC) designed as a multipurpose detector for a wide range of energies. It is motivated by the requirements of neutrino detection [9] and light dark matter searches [12] and builds on the considerable investment in liquid noble gas detectors over the last decade (ICARUS, MicroBooNE, SBND, ProtoDUNE, and

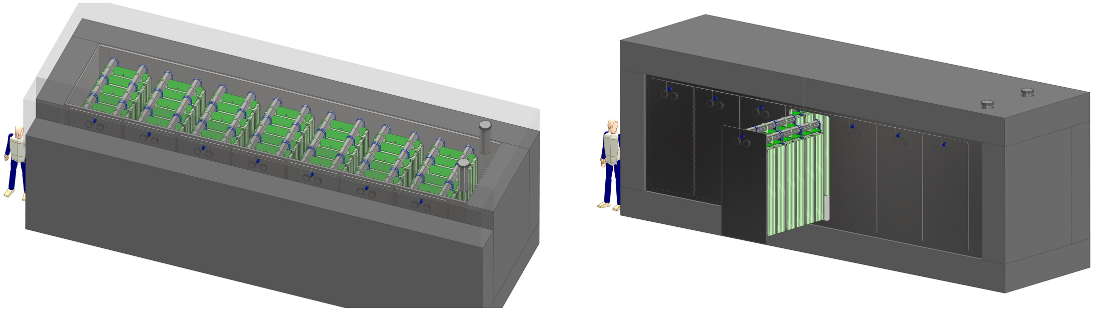

FIG. 19. Layout of the FLArE baseline design. The detector is shown with the 3×7 modular segmentation. Three TPC modules are also shown withdrawn horizontally from the cryostat.

various components of DUNE). Liquid argon as an active medium allows one to precisely determine particle identification, track angle, and kinetic energy from tens of MeV to many hundreds of GeV, thus covering both dark matter scattering and high-energy LHC neutrinos. It also provides complementarity to other FPF detectors (such as emulsion detectors or magnetic spectrometers) that are more tuned for single-purpose measurements.

FLArE is expected to see about 25-50 high-energy neutrino events/ton/fb^{-1} of collisions, providing the opportunity to measure the neutrino fluxes and cross-section for all three flavors. The identification of tau neutrinos is a particularly challenging task requiring detailed simulations and reconstruction studies, but could in principle be achieved with high spatial and kinematic resolution. In addition, the large active volume and millimeter-level spatial resolution, along with excellent calorimetry, provide sensitivity to dark matter searches via electron scattering, as mentioned in Sec. I.

Fig. 19 shows the current baseline design for FLArE. A significant engineering effort has been carried out to define the detector geometry, cryogenics, and integration within the FPF cavern. The latest configuration is based on a single-wall 8.8 m × 2.0 m × 2.4 m foam-insulated cryostat. The TPC is segmented in 21 modules, arranged in a 3×7 configuration. Each TPC module (1.0 m × 0.6 m × 1.8 m) is divided into two volumes by a central cathode, with an anode at either end, resulting in 42 separate 30 cm drift volumes. The modularity is needed for two main reasons: first, the muon rate at the FPF (Fig. 14) is sufficiently high that the space charge intensity requires a short gap (< 50 cm); and second, the trigger capability is enhanced by compartmentalizing the intense scintillation light from liquid argon. The total liquid argon fiducial (active) mass in this configuration is approximately 10 tons (30 tons).

Given the limited height in the current design of the FPF cavern, the vertical insertion of the TPC modules into the cryostat is not possible. The insertion proceeds horizontally through doors on the side of the cryostat in a ”filing cabinet” concept. A similar solution has been already successfully demonstrated in the EXO cryostat [115]. Each set of three TPC modules is mechanically supported via cantilevered beams by one of the cold doors. At the same time the door hosts the high-voltage feedthrough and flanges for readout electronics power and signal, as shown in Fig. 20. These assemblies can be easily transported into the cavern via wheeled carts. A custom machine holding the outer warm side of the door can then align and insert them, sealing the door against the cryostat itself. This procedure simplifies the installation and offers the possibility to extract single assemblies for maintenance or upgrades.

Upon consultation with the CERN cryogenics experts, the cryogenic system for FLArE has gone through a substantial redesign. As shown in Fig. 13, the western side of the FPF cavern is now reserved for some of the cryogenic infrastructure, including storage tanks for liquid argon,

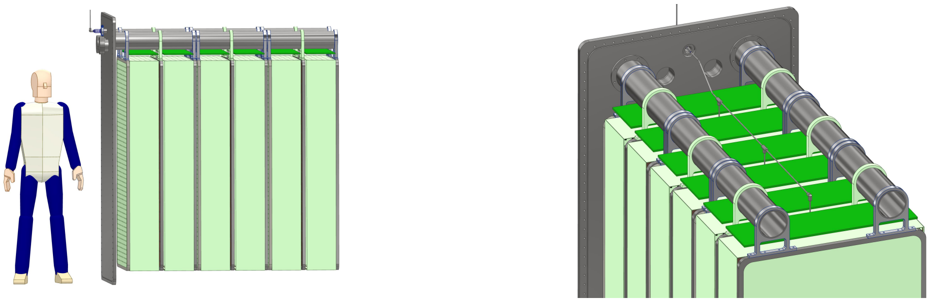

FIG. 20. Left: TPC assembly with three TPC modules hanging from the cold door via cantilevered beams. Right: Inner view showing a conceptual high-voltage connection scheme to the cathode planes.

and nitrogen and a Turbo-Brayton LN2 condenser, which is a commercial unit that reduces the need to provide LN2 for cooling continuously. These facilities are kept away from the detectors to reduce noise or vibration. The proximity cryogenics near the FLArE detector will simply consist of condensers and circulation systems for purity, all based on well known techniques from protoDUNE or ICARUS. Briefly, LAr will be delivered at the surface and then filled in the tank underground, and the underground tank will serve both as temporary storage and remain cold to receive the liquid from the detector in case of an emergency. LN2 will be delivered at the surface and filled in the Turbo-Brayton system to keep the detector and the LAr cold.

The anode charge readout will be pixelated. Preliminary simulations suggest that a 5 mm pixel size will satisfy the spatial resolution requirements for track reconstruction and particle identification, as well as being reasonable from the point of view of electron diffusion, which inevitably diminishes the advantages of finer spacing. At a typical drift field of 500 V/cm, this translates to $\sim 20,000$ electrons per pixel from minimum-ionizing muons and corresponds to a 30:1 signal-to-noise ratio assuming a total electronic noise of 500 electron equivalent noise charge (ENC). Concerning the electronics, two approaches are being considered: the LArPix ASIC [116] developed for the DUNE Near Detector and the Q-Pix [117] readout scheme. Given the high number of pixels, 7200 per anode plane, careful considerations need to be taken to avoid an excessive heat load into the liquid. For instance, a proposed option to reduce the channel count consists of using a strip-based readout for the non-fiducial outer regions of the detector.

An alternative readout design for FLArE is based on a 3D optical TPC similar to that developed within the ARIADNE programme. The ARIADNE approach utilises the 1.6 ns timing resolution and native 3D raw data of a Timepix3 camera to image the wavelength-shifted secondary scintillation light generated by a novel glass THGEM (THick Gaseous Electron Multiplier) within the gas phase of a dual-phase LArTPC [118, 119]. In this scenario, charge is drifted 1.8 m vertically towards an extraction grid situated below the liquid level where they are transferred to the gas phase and subsequently amplified using a THGEM. The drift charge multiplication produces secondary scintillation light which is wavelength-shifted and imaged by Timepix3 cameras, providing a time sequence of 2D snapshots of the detector. This readout technology was successfully operated in a 2 m × 2 m prototype at the CERN Neutrino Platform [120]. FLArE would be instrumented with 56 TimePix3 cameras, installed externally at cryostat view-ports. This design would lower the overall cost by eliminating the charge readout in favor of commercial and decoupled external devices, making it a valuable alternative to the more traditional TPC design.

One of the key requirements for FLArE is the ability to fully contain neutrino events and reconstruct their kinematics to identify the neutrino type. While the transverse size of the TPC (1.8 m) was tuned with simulations for energy containment, energetic muons and a significant

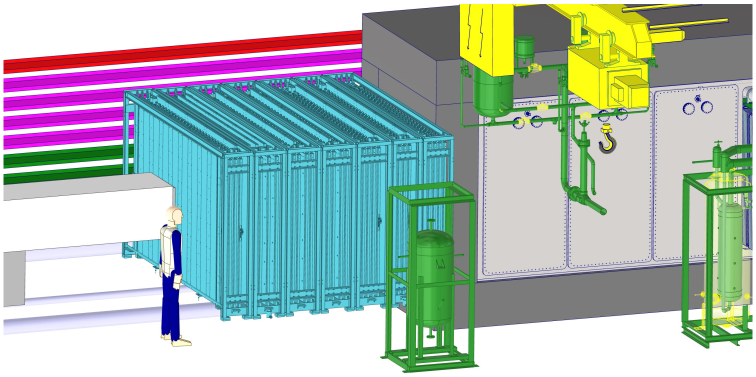

FIG. 21. Preliminary design of the magnetized hadron/muon calorimeter downstream of the FLArE cryostat in the FPF cavern. The implementation is based on the Baby MIND concept [121].

fraction of hadronic showers still escape the liquid argon volume along the line of sight. To improve energy containment and muon tagging, a magnetized hadron calorimeter/muon spectrometer is envisioned downstream of the TPC. Fig. 21 shows a possible design based on the Baby MIND neutrino detector concept employed in the WAGASCI experiment [121]. It consists of magnetized iron plates interleaved with scintillator modules that measure the particle position and the curvature of the track along the assembly. The clever magnetization scheme of the iron plates [122] allows one to achieve a 1.5 T field inside the iron module with minimum stray field and operating current. This configuration avoids the need of bulky return yokes and cryogenic cooling, greatly easing its integration. Simulations are in progress to define the number and size of the plates for optimal containment and muon tagging efficiency. In addition, the synergy with the FASER2 magnetic spectrometer is also being investigated, since it is expected to provide up to $45-55\%$ acceptance for high-energy muons, depending on the final magnet design.

Overall FLArE will be an excellent neutrino detector that plays well with the FPF physics opportunities. Although additional R&D is needed, the technical design is maturing quickly, and there is sufficient time and expertise available to complete all remaining tasks successfully within the FPF time frame.

VII. INTERNATIONAL PARTNERSHIPS AND ORGANIZATION

The FPF and the forward physics detector collaborations will follow the best governance practices established by other major collaborations such as ATLAS, CMS, DUNE, etc. The scale of the FPF enterprise is much smaller than these collaborations, and so we will need to adjust the governance and coordination practices to be suitable. We will also look at other models for this coordination, such as the LHCb or R&D collaborations at CERN. An important difference between these major collaborations and the FPF community is the possibility of several independent FPF scientific collaborations using the same facility and sharing resources. All of these collaborations will be international in nature.

Three of the proposed experiments, FASER2, FASERν2, and FORMOSA, have pathfinder projects that are already installed and running at the LHC: FASER, FASERν, and milliQan, respectively. FASER has already placed world-leading bounds on dark photons [123] and axion-like particles [124], FASERν has detected both electron and muon collider neutrinos [27] and measured their cross sections at TeV energies for the first time [30], and milliQan has already placed world-leading bounds on mCPs [114]. These results highlight the physics potential of the forward region, even with modest luminosities and small experiments. The collaborations behind the existing experiments are creating a community for this science that will serve all experiments in the FPF.

Currently, the broader FPF experimental and theoretical community is approximately ∼400 strong; see the list of contributors to Ref. [10]. This community and additional scientists are expected to form the collaborations needed for the FPF experiments. The community is currently dominated by scientists from Europe, US, and Japan. Discussions to obtain R&D support from their respective agencies and institutions are in progress.

Along with the conceptual design report for the experiments and the facility, the community will propose a management structure under the guidance of CERN. This structure will need to have a strong technical coordination team to construct the facility according to the scientific and engineering requirements and also to install the detectors. Each of the scientific collaborations will have representation in the technical coordination team and will provide scientific resources as needed. Each collaboration will also seek coordination and resolution of overlapping requirements.

We expect the scientific collaborations to act independently to promote their respective science and detectors, and seek collaborators from CERN and the broader international particle physics communities. CERN has a longstanding procedure for accommodating such new collaborators, mainly from Europe and North America. For the FPF, we will attempt to broaden this to other parts of the world, especially in Asia, Africa, and the Americas. Such expansion will be welcome to inject new resources into this effort. Fortunately, the current program for forward physics has created a core community that is centered around the experiments FASER, FASERν, and milliQan. This community is expected to lead the proposals for the FPF suite of experiments, but additional proposals that enhance the physics capabilities of the FPF are, of course, welcome.

Below we make some remarks about the status of the collaborations for each of the constituent experiments along with what is needed for further expansion:

- FASER2: The current FASER Collaboration has more than 110 members from 28 institutions in 11 countries [125]. FASER is a magnetized spectrometer (using permanent dipole magnets) that is housed in a service tunnel forward of ATLAS. It started taking data in Run 3. The FASER Collaboration is expected to form the core of the FASER2 effort. FASER2 will require a much larger effort towards an appropriate spectrometer magnet and a larger tracking system that can handle the trigger rates from HL-LHC. It also needs careful integration into the FPF hall and with the other experiments. The Collaboration will need to expand to bring in the appropriate technical expertise and resources for the larger effort.
- FASERν2: The FASERν2 collaboration will largely be made up from the existing FASERν experts who are part of the 110-person FASER Collaboration. The expertise on emulsion is mostly concentrated in Japan, where there is deep expertise and a strong tradition in using emulsion-based detectors for neutrino physics. Japan has the leading facilities for emulsion gel production and for the scanning of the emulsion films after exposure, and these will both be used in the FASERν2 operations.
- FLArE: FLArE is based on the liquid argon technology developed for the FNAL short baseline program, as well as DUNE. The FLArE collaboration will be based on the current working groups, which have approximately ∼50 participants, equally divided between US and European collaborators. The collaboration has received support from a private foundation, and a US national laboratory- (BNL-)directed R&D program. Because of the recent investment in DUNE prototypes, only limited and well-targeted R&D is needed for FLArE. Specifically, the readout electronics and pixel readout will need optimization for spatial resolution and dynamic range,

however the majority of the design can be simply adapted from the DUNE ND-LAR design. Furthermore, trigger strategies will need to be developed for the FLArE geometry. At the moment, the collaboration has enough resources and person power to provide a physics proposal and a well-considered conceptual design. A modest-sized international collaboration (∼100 collaborators) with appropriate experience will have to be developed by the time of the technical design report in a few years.

- FORMOSA: FORMOSA would be based on the existing milliQan Collaboration with 29 members from 10 institutions in 5 countries [126]. The FORMOSA concept is based on well-known technologies that require limited R&D and is focused on mCPs. Alterations and improvements to the design to substantially improve the detector sensitivity, such as through the use of alternative scintillator material, are under study, and the collaboration is expected to grow accordingly.

VIII. SCHEDULE, BUDGET, AND TECHNICAL COORDINATION

A very preliminary budget and schedule is being assembled for the FPF facility and the component experiments; this has been discussed in successive FPF workshops [5–7]. The costs are in several separate groups, as indicated in Table I. For this report we provide new cost numbers compared to the US-based estimates in Ref. [127]: the civil construction design has been improved, providing more space and creating a section of the tunnel for cryogenic infrastructure away from the experiments [90], and the overall concepts for installation of all detectors and facilities have been improved.

The cost for the civil construction and the outfitting was provided by the CERN civil engineering group and the technical infrastructure groups, respectively. They reviewed the initial experimental requirements for the needed location, underground space, and services, and performed a Class 4 estimate [128]. According to international standards of conventional construction, a Class 4 estimate has a range of −30% to +50% around the point estimate. The outfitting includes electrical service, as well as safety, ventilation, transportation, and lift services that are needed for the facility. Obviously, the facility costs depend on the experimental requirements, which are expected to evolve as we progress towards a technical design.

The costs for the experimental program were assembled by the proponents. These core costs are shown in Table I for the FPF experiments. The costs for FASER2 are dominated by the proposed magnetic spectrometer systems. For FASERν2, the costs are dominated by the production and handling of emulsion. The international division of scope for components for these projects is currently not well defined, and therefore these core costs are provided without labor, overhead, contingency, and additional factors that must be used for a full cost estimate according to the rules of each national sponsor.

FLArE and FORMOSA have substantial US portions; US cost estimates tend to include preliminary estimates for engineering, management, labor, overhead, and contingency factors. These are not included in Table I so that uniform core costs can be presented for each experimental project.

FORMOSA is a conventional plastic scintillator-based detector with PMT readout. The estimate includes mostly off-the-shelf parts and conventional assembly. The number presented is for the more expensive commercial option for the readout electronics. The FLArE estimate is based on the DUNE ND design with some modifications and includes a scintillator/steel hadron calorimeter using the Baby-MIND detector as a model [121]. The design will require targeted R&D for the TPC electronics, a sophisticated photon sensor system, trigger electronics, and clean assembly. Granular details for the FLArE and FORMOSA costs including other factors are available at a pre-conceptual level. These costs will be refined and further improved as we proceed to the conceptual design.

Component	Approximate Cost	Comments
Facility Costs		
FPF civil construction	35.3 MCHF	Construction of shaft and cavern
FPF outfitting costs	10.0 MCHF	Electrical, safety, and integration
Cryogenic infrastructure	3.8 MCHF	Cryogen storage and cooling systems
Total	**49.1 MCHF**	Includes integration for infrastructure
Experiment Costs		Core costs only
FASER2	11.6 MCHF	3+3 tracker layers, SAMURAI-style magnet, dual-readout calorimeter
FASERν2	15.9 MCHF	Tungsten target, scanning system, emulsion films (10 replacements), interface detector
FLArE	10.8 MCHF	Cryostat, proximity cryogenics, detectors
FORMOSA	2.3 MCHF	Plastic scintillator, PMTs, readout
Total	**40.6 MCHF**	Core cost experimental program

TABLE I. Cost for components of the FPF and the experimental program. Costs of the infrastructure at CERN are Class 4 estimates according to international standards; they have a range from −30% to +50%. The costs for experimental components are estimated as core costs, which consist of direct costs of materials and contracts only. Each core cost was computed with conservative technical choices; as new ideas and designs are considered, the costs are expected to change.

A few additional comments are necessary for the project costs:

- The cost for FASERν2 includes the cost of replacing the emulsion films 10 times. These costs could change over time or be absorbed in the costs of detector operations.
- The baseline for FLArE is now a single walled foam insulated cryostat that is opened on the side for installation. This design has been verified, but needs detailed reviews from laboratory experts. The cost should be considered very preliminary; it represents a substantial savings compared to a membrane style cryostat. The costs presented are for a pixel-style readout, but a very significant option for FLArE is the ARIADNE optical readout option. The cost of this option is dominated by the Timpix3 camera readout, but could be lower than the pixel option.
- Upon consultation with CERN experts, some of the cryogenic infrastructure has been separated from the experimental costs and included in the upper portion of the table. The proximity cryogenics, which includes circulation and purification systems, is included in the FLArE experimental costs.
- Transport services will be needed for installation of large pieces such as the FASER2 magnet and the FLArE cryostat. In addition, services will be needed for transporting the emulsion detector periodically. The cryostat/cryogenics and additional infrastructure design and costs clearly need to be coordinated and shared with CERN. This process of coordination has started only recently.
- The cost for experiments does not include engineering, labor, project management, contingency, and the research support that will be needed. Obviously, for an effort of this size, considerable support will be needed by a collaboration for students, postdocs, travel, and R&D. This is not included in the table. We estimate the total size of the collaboration to range from 250 to 350 people with corresponding annual support from the national agencies.

The cost estimate for the FPF and its experiments will be refined in successive stages and reviews, as normally done for large acquisitions. We expect the review process to be defined by

Year	2024	2025	2026	2027	2028	2029	2030	2031	2032	2033
(HL-)LHC Nominal Schedule	Run 3	Run 3	Run 3 / LS 3	LS 3	LS 3	LS 3	LS 3 / Run 4	Run 4	Run 4	Run 4
FPF Milestones	Pre-CDR and physics proposal	R&D and prototype detectors	CDR, long lead items, magnet	Start of civil construction, TDR for detectors	Detector construction start	Major equipment acq.	End of civil construction, Install services	Detector install	Detector commissioning, physics start	Physics running all detectors
Experiment Core Costs (kCHF)		154	1275	3473	7257	11220	9503	6978	741	

TABLE II. Proposed funding profile for the FPF experimental program using the core cost numbers from Table I. The infrastructure cost profile is being developed. The approval and cost rules will be different for the different sponsors who are proposed to contribute to this overall profile. Nevertheless, for the purpose of this illustration, the profile is shown in as-spent funds in a single currency.

CERN, as the host lab, and the leading funding organizations that will be involved, such as the UK-STFC, US DOE and NSF, and Japanese JSPS. Clearly, additional steps are needed to better define the scope of the facility and the constituent physics experiments. The FPF community will continue with its working group activities and the FPF workshops. Detailed simulation activities have commenced and have provided critical information on detector sizes and depths needed for good efficiency and energy containment for various types of neutrino interactions, as well as for sensitive searches for the many possible BSM scenarios. The CERN accelerator and radiation protection groups have contributed immensely by providing detailed simulations of the muon rates. These simulation activities will require appropriate levels of support to develop the detailed requirements needed for a conceptual design report.

Table II has the proposed approximate funding profile using the current understanding of the cost estimates for components. In the following we provide the constraints used for assembling this funding profile:

- Table II includes some milestones and the nominal HL-LHC schedule. Any FPF construction must be coordinated with the HL-LHC, so that the civil construction and demands on personnel do not interfere with LHC operations.
- The CERN radiation protection group has concluded that the FPF can be accessed during LHC operations with appropriate controls for radiation safety. This will allow detector installation to proceed during Run 4.
- An important constraint is that detector construction, installation, and commissioning must happen before Run 4 concludes. This is quite important for the scientific productivity of the FPF and organization of the FPF community.
- We assume that the funding profile for the CERN infrastructure will follow the appropriate profile to allow start of detector installation in the 2030-2031 time frame.
- Full detector construction funding is assumed to start in 2027. However, critical development, such as the FASER2 magnet systems and FLArE cryostat, may require funding ahead of this date. Planning and integration of the FPF program will require excellent technical coordination with leadership from the host laboratories.

ACKNOWLEDGMENTS

We are grateful to Roshan Mammen Abraham, Max Fieg, and Jinmian Li for providing data for discovery reach plots. JA and ST are supported by the National Science Centre, Poland, research grant No. 2021/42/E/ST2/00031. JA is also partially supported from the STER programme – Internationalisation of Doctoral Schools by NAWA. The work of LAA is supported by the U.S. National Science Foundation grant PHY-2412679. The work of AJB is funded in part through STFC grants ST/R002444/1 and ST/S000933/1. The work of BB is supported by U.S. Department of Energy grant DE–SC-0007914. The work of JB, MVD, SL, MV, and WW is supported in part by Heising-Simons Foundation Grant 2022-3319. The work of MC is supported in part by U.S. Department of Energy grant DE-SC0009999. The work of JLF and TM is supported in part by U.S. National Science Foundation grants PHY-2111427 and PHY-2210283. The work of JLF is supported in part by Simons Investigator Award #376204, Heising-Simons Foundation Grants 2019-1179 and 2020-1840, and Simons Foundation Grant 623683. The work of CSH is supported in part by U.S. Department of Energy Grant DE-SC0011726. The work of FK is supported by the Deutsche Forschungsgemeinschaft under Germany's Excellence Strategy – EXC 2121 Quantum Universe – 390833306. The work of JM is supported by the Royal Society grant URF\R1\201519 and STFC grant ST/W000512/1. The work of JR is partially supported by NWO, the Dutch Research Council, and by the Netherlands eScience Center (NLeSC). The work at BNL is under U.S. Department of Energy contract No. DE-SC-0012704.

Appendix A: Civil Engineering Costs

Fig. 22 shows a detailed breakdown of the CE costs. This is for the point estimate of 35.3 MCHF. As a Class 4 estimate, the range is from −30% to +50%.

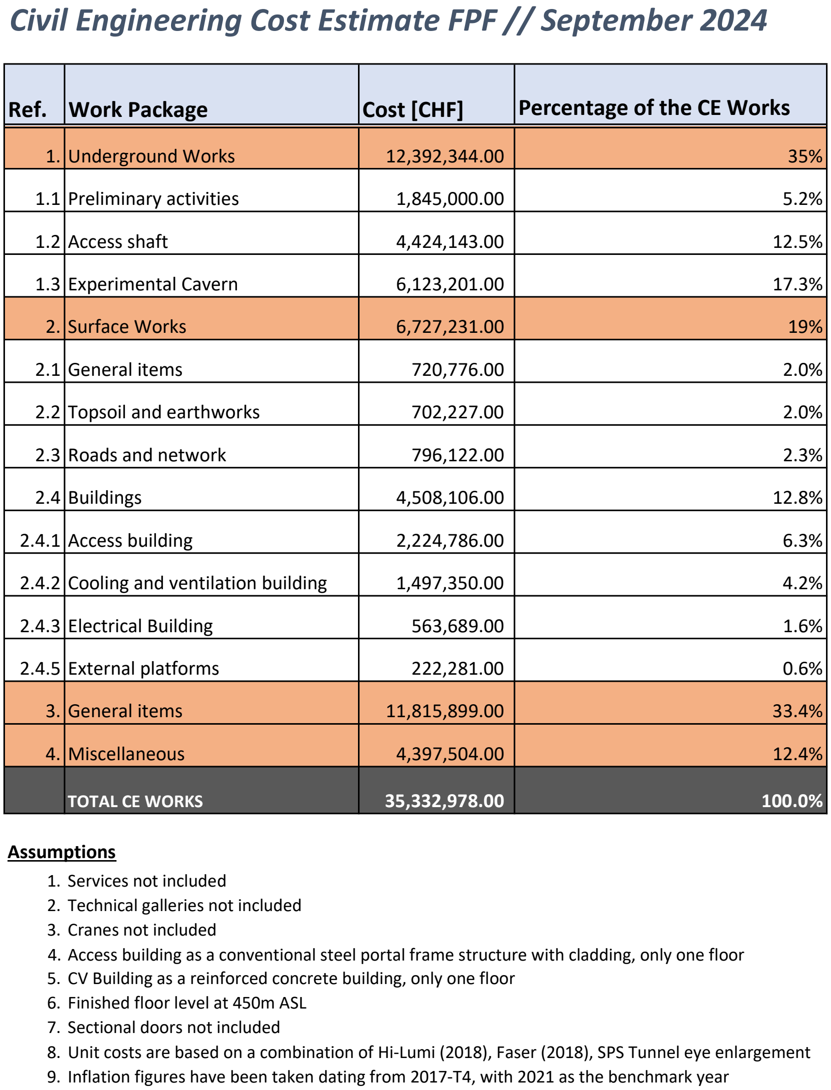

Civil Engineering Cost Estimate FPF // September 2024

Ref.	Work Package	Cost [CHF]	Percentage of the CE Works
1.	Underground Works	12,392,344.00	35%
1.1	Preliminary activities	1,845,000.00	5.2%
1.2	Access shaft	4,424,143.00	12.5%
1.3	Experimental Cavern	6,123,201.00	17.3%
2.	Surface Works	6,727,231.00	19%
2.1	General items	720,776.00	2.0%
2.2	Topsoil and earthworks	702,227.00	2.0%
2.3	Roads and network	796,122.00	2.3%
2.4	Buildings	4,508,106.00	12.8%
2.4.1	Access building	2,224,786.00	6.3%
2.4.2	Cooling and ventilation building	1,497,350.00	4.2%
2.4.3	Electrical Building	563,689.00	1.6%
2.4.5	External platforms	222,281.00	0.6%
3.	General items	11,815,899.00	33.4%
4.	Miscellaneous	4,397,504.00	12.4%
	TOTAL CE WORKS	**35,332,978.00**	**100.0%**

Assumptions

1. Services not included
2. Technical galleries not included
3. Cranes not included
4. Access building as a conventional steel portal frame structure with cladding, only one floor
5. CV Building as a reinforced concrete building, only one floor
6. Finished floor level at 450m ASL
7. Sectional doors not included
8. Unit costs are based on a combination of Hi-Lumi (2018), Faser (2018), SPS Tunnel eye enlargement
9. Inflation figures have been taken dating from 2017-T4, with 2021 as the benchmark year

FIG. 22. A detailed breakdown of the costs of the baseline CE works.

[1] "Forward Physics Facility Kickoff Meeting." `https://indico.cern.ch/event/955956`, 9-10 November 2020.

[2] "2nd Forward Physics Facility Meeting (FPF2)." `https://indico.cern.ch/event/1022352`, 27-28 May 2021.

[3] "3rd Forward Physics Facility Meeting (FPF3)." `https://indico.cern.ch/event/1076733`, 25-26 October 2021.

[4] "4th Forward Physics Facility Meeting (FPF4)." `https://indico.cern.ch/event/1110746`, 31 January-1 February 2022.

[5] "5th Forward Physics Facility Meeting (FPF5)." `https://indico.cern.ch/event/1196506`, 15-16 November 2022.

[6] "6th Forward Physics Facility Meeting (FPF6)." `https://indico.cern.ch/event/1275380`, 8-9 June 2023.

[7] "7th Forward Physics Facility Meeting (FPF7)." `https://indico.cern.ch/event/1358966`, 29 February - 1 March 2024.

[8] "Forward Physics Facility Theory Workshop." `https://indico.cern.ch/event/1296658`, 18-19 September 2024.

[9] L. A. Anchordoqui *et al.*, "The Forward Physics Facility: Sites, experiments, and physics potential," *Phys. Rept.* **968** (2022) 1–50, `arXiv:2109.10905 [hep-ph]`.

[10] J. L. Feng *et al.*, "The Forward Physics Facility at the High-Luminosity LHC," *J. Phys. G* **50** (2023) no. 3, 030501, `arXiv:2203.05090 [hep-ex]`.

[11] **FASER** Collaboration, A. Ariga *et al.*, "Letter of Intent for FASER: ForwArd Search ExpeRiment at the LHC," `arXiv:1811.10243 [physics.ins-det]`.

[12] B. Batell, J. L. Feng, and S. Trojanowski, "Detecting Dark Matter with Far-Forward Emulsion and Liquid Argon Detectors at the LHC," *Phys. Rev. D* **103** (2021) no. 7, 075023, `arXiv:2101.10338 [hep-ph]`.

[13] S. Foroughi-Abari, F. Kling, and Y.-D. Tsai, "Looking forward to millicharged dark sectors at the LHC," *Phys. Rev. D* **104** (2021) no. 3, 035014, `arXiv:2010.07941 [hep-ph]`.

[14] A. Berlin and F. Kling, "Inelastic Dark Matter at the LHC Lifetime Frontier: ATLAS, CMS, LHCb, CODEX-b, FASER, and MATHUSLA," *Phys. Rev. D* **99** (2019) no. 1, 015021, `arXiv:1810.01879 [hep-ph]`.

[15] K. R. Dienes, J. L. Feng, M. Fieg, F. Huang, S. J. Lee, and B. Thomas, "Extending the discovery potential for inelastic-dipole dark matter with FASER," *Phys. Rev. D* **107** (2023) no. 11, 115006, `arXiv:2301.05252 [hep-ph]`.

[16] R. Alemany *et al.*, "Summary Report of Physics Beyond Colliders at CERN," `arXiv:1902.00260 [hep-ex]`.

[17] B. Batell, J. L. Feng, A. Ismail, F. Kling, R. M. Abraham, and S. Trojanowski, "Discovering dark matter at the LHC through its nuclear scattering in far-forward emulsion and liquid argon detectors," *Phys. Rev. D* **104** (2021) no. 3, 035036, `arXiv:2107.00666 [hep-ph]`.

[18] B. Batell, J. L. Feng, M. Fieg, A. Ismail, F. Kling, R. M. Abraham, and S. Trojanowski, "Hadrophilic dark sectors at the Forward Physics Facility," *Phys. Rev. D* **105** (2022) no. 7, 075001, `arXiv:2111.10343 [hep-ph]`.

[19] F. Kling, J.-L. Kuo, S. Trojanowski, and Y.-D. Tsai, "FLArE up dark sectors with EM form factors at the LHC forward physics facility," *Nucl. Phys. B* **987** (2023) 116103, `arXiv:2205.09137 [hep-ph]`.

[20] J. L. Feng, J. Li, X. Liao, J. Ni, and J. Pei, "Discovering quirks through timing at FASER and future forward experiments at the LHC," *JHEP* **06** (2024) 197, `arXiv:2404.13814 [hep-ph]`.

[21] B. Batell, M. Low, E. T. Neil, and C. B. Verhaaren, "Review of Neutral Naturalness," in *Snowmass 2021*. 3, 2022. `arXiv:2203.05531 [hep-ph]`.

[22] A. De Rujula and R. Ruckl, "Neutrino and muon physics in the collider mode of future accelerators," in *SSC Workshop: Superconducting Super Collider Fixed Target Physics*, pp. 571–596. 5, 1984. `http://inspirehep.net/record/204753/files/p571.pdf`.

[23] **FASER** Collaboration, H. Abreu *et al.*, "Technical Proposal: FASERnu," `arXiv:2001.03073 [physics.ins-det]`.

[24] **SND@LHC** Collaboration, G. Acampora *et al.*, "SND@LHC: The Scattering and Neutrino Detector at the LHC," `arXiv:2210.02784 [hep-ex]`.

[25] **FASER** Collaboration, Petersen, Brian, "First Physics Results from the FASER Experiment." `https://indico.in2p3.fr/event/29681/contributions/122474/attachments/76425/110931/05-BPetersen-v1.pdf`, 19 March 2023.

[26] **SND@LHC** Collaboration, Zaffaroni, Ettore, "Results of SND@LHC." `https://indico.in2p3.fr/event/29681/contributions/122476/attachments/76427/110933/07-EZaffaroni-v1-public.pdf`, 19 March 2023.

[27] **FASER** Collaboration, H. Abreu *et al.*, "First Direct Observation of Collider Neutrinos with FASER at the LHC," *Phys. Rev. Lett.* **131** (2023) no. 3, 031801, `arXiv:2303.14185 [hep-ex]`.

[28] **Particle Data Group** Collaboration, P. A. Zyla *et al.*, "Review of Particle Physics," *PTEP* **2020** (2020) no. 8, 083C01.

[29] **IceCube** Collaboration, M. G. Aartsen *et al.*, "Measurement of the multi-TeV neutrino cross section with IceCube using Earth absorption," *Nature* **551** (2017) 596–600, `arXiv:1711.08119 [hep-ex]`.

[30] **FASER** Collaboration, R. Mammen Abraham *et al.*, "First Measurement of ν_e and ν_μ Interaction Cross Sections at the LHC with FASER's Emulsion Detector," *Phys. Rev. Lett.* **133** (2024) no. 2, 021802, `arXiv:2403.12520 [hep-ex]`.

[31] T. Pierog, I. Karpenko, J. M. Katzy, E. Yatsenko, and K. Werner, "EPOS LHC: Test of collective hadronization with data measured at the CERN Large Hadron Collider," *Phys. Rev. C* **92** (2015) no. 3, 034906, `arXiv:1306.0121 [hep-ph]`.

[32] L. Buonocore, F. Kling, L. Rottoli, and J. Sominka, "Predictions for neutrinos and new physics from forward heavy hadron production at the LHC," *Eur. Phys. J. C* **84** (2024) no. 4, 363, `arXiv:2309.12793 [hep-ph]`.

[33] F. Kling and L. J. Nevay, "Forward neutrino fluxes at the LHC," *Phys. Rev. D* **104** (2021) no. 11, 113008, `arXiv:2105.08270 [hep-ph]`.

[34] F. Kling, T. Mäkelä, and S. Trojanowski, "Investigating the fluxes and physics potential of LHC neutrino experiments," *Phys. Rev. D* **108** (2023) no. 9, 095020, `arXiv:2309.10417 [hep-ph]`.

[35] A. Falkowski, M. González-Alonso, J. Kopp, Y. Soreq, and Z. Tabrizi, "EFT at FASERν," *JHEP* **10** (2021) 086, `arXiv:2105.12136 [hep-ph]`.

[36] F. Kling, "Probing light gauge bosons in tau neutrino experiments," *Phys. Rev. D* **102** (2020) no. 1, 015007, `arXiv:2005.03594 [hep-ph]`.

[37] L. A. Anchordoqui, I. Antoniadis, K. Benakli, J. Cunat, and D. Lüst, "Searching for neutrino-modulino oscillations at the Forward Physics Facility," *Phys. Lett. B* **850** (2024) 138530, `arXiv:2308.11476 [hep-ph]`.

[38] L. A. Anchordoqui, I. Antoniadis, K. Benakli, J. Cunat, and D. Lüst, "SUSY at the FPF," `arXiv:2410.16342 [hep-ph]`.

[39] R. Mammen Abraham, S. Foroughi-Abari, F. Kling, and Y.-D. Tsai, "Neutrino Electromagnetic Properties and the Weak Mixing Angle at the LHC Forward Physics Facility," `arXiv:2301.10254 [hep-ph]`.

[40] A. Ismail, R. Mammen Abraham, and F. Kling, "Neutral current neutrino interactions at FASERν," *Phys. Rev. D* **103** (2021) no. 5, 056014, `arXiv:2012.10500 [hep-ph]`.

[41] K. J. Kelly, F. Kling, D. Tuckler, and Y. Zhang, "Probing neutrino-portal dark matter at the Forward Physics Facility," *Phys. Rev. D* **105** (2022) no. 7, 075026, `arXiv:2111.05868 [hep-ph]`.

[42] W. Altmannshofer, T. Mäkelä, S. Sarkar, S. Trojanowski, K. Xie, and B. Zhou, "Discovering neutrino tridents at the Large Hadron Collider," *Phys. Rev. D* **110** (2024) no. 7, 072018, `arXiv:2406.16803 [hep-ph]`.

[43] R. Gauld and J. Rojo, "Precision determination of the small-x gluon from charm production at LHCb," *Phys. Rev. Lett.* **118** (2017) no. 7, 072001, `arXiv:1610.09373 [hep-ph]`.

[44] J. Rojo, "Deep-Inelastic Scattering with LHC Neutrinos," in *31st International Workshop on Deep-Inelastic Scattering and Related Subjects*. 7, 2024. `arXiv:2407.06731 [hep-ph]`.

[45] **PROSA** Collaboration, O. Zenaiev, M. V. Garzelli, K. Lipka, S. O. Moch, A. Cooper-Sarkar, F. Olness, A. Geiser, and G. Sigl, "Improved constraints on parton distributions using LHCb, ALICE and HERA heavy-flavour measurements and implications for the predictions for prompt atmospheric-neutrino fluxes," *JHEP* **04** (2020) 118, `arXiv:1911.13164 [hep-ph]`.

[46] P. Duwentäster, V. Guzey, I. Helenius, and H. Paukkunen, "Proton PDFs with nonlinear corrections from gluon recombination," *Phys. Rev. D* **109** (2024) no. 9, 094004, `arXiv:2312.12993 [hep-ph]`.

[47] A. Bhattacharya, F. Kling, I. Sarcevic, and A. M. Stasto, "Forward neutrinos from charm at the Large Hadron Collider," *Phys. Rev. D* **109** (2024) no. 1, 014040, `arXiv:2306.01578 [hep-ph]`.

[48] **NNPDF** Collaboration, R. D. Ball, A. Candido, J. Cruz-Martinez, S. Forte, T. Giani, F. Hekhorn, K. Kudashkin, G. Magni, and J. Rojo, "Evidence for intrinsic charm quarks in the proton," *Nature* **608** (2022) no. 7923, 483–487, `arXiv:2208.08372 [hep-ph]`.

[49] R. Maciula and A. Szczurek, "Far-forward production of charm mesons and neutrinos at forward physics facilities at the LHC and the intrinsic charm in the proton," *Phys. Rev. D* **107** (2023) no. 3, 034002, `arXiv:2210.08890 [hep-ph]`.

[50] J. M. Cruz-Martinez, M. Fieg, T. Giani, P. Krack, T. Mäkelä, T. R. Rabemananjara, and J. Rojo, "The LHC as a Neutrino-Ion Collider," *Eur. Phys. J. C* **84** (2024) no. 4, 369, `arXiv:2309.09581 [hep-ph]`.

[51] E. Hammou, Z. Kassabov, M. Madigan, M. L. Mangano, L. Mantani, J. Moore, M. M. Alvarado, and M. Ubiali, "Hide and seek: how PDFs can conceal new physics," *JHEP* **11** (2023) 090, `arXiv:2307.10370 [hep-ph]`.

[52] Z. Kassabov, M. Madigan, L. Mantani, J. Moore, M. Morales Alvarado, J. Rojo, and M. Ubiali, "The top quark legacy of the LHC Run II for PDF and SMEFT analyses," *JHEP* **05** (2023) 205, `arXiv:2303.06159 [hep-ph]`.

[53] M. van Beekveld, S. Ferrario Ravasio, E. Groenendijk, P. Krack, J. Rojo, and V. S. Sánchez, "A Phenomenological Analysis of LHC Neutrino Scattering at NLO Accuracy Matched to Parton Showers," `arXiv:2407.09611 [hep-ph]`.

[54] M. Fieg, F. Kling, H. Schulz, and T. Sjöstrand, "Tuning pythia for forward physics experiments," *Phys. Rev. D* **109** (2024) no. 1, 016010, `arXiv:2309.08604 [hep-ph]`.

[55] S. Ferrario Ravasio, R. Gauld, B. Jäger, A. Karlberg, and G. Zanderighi, "An event generator for neutrino-induced Deep Inelastic Scattering and applications to neutrino astronomy," `arXiv:2407.03894 [hep-ph]`.

[56] L. Buonocore, G. Limatola, P. Nason, and F. Tramontano, "An event generator for Lepton-Hadron deep inelastic scattering at NLO+PS with POWHEG including mass effects," *JHEP* **08** (2024) 083, `arXiv:2406.05115 [hep-ph]`.

[57] R. Abdul Khalek *et al.*, "Science Requirements and Detector Concepts for the Electron-Ion Collider: EIC Yellow Report," *Nucl. Phys. A* **1026** (2022) 122447, `arXiv:2103.05419 [physics.ins-det]`.

[58] M. Guzzi, T. J. Hobbs, K. Xie, J. Huston, P. Nadolsky, and C. P. Yuan, "The persistent nonperturbative charm enigma," *Phys. Lett. B* **843** (2023) 137975, `arXiv:2211.01387 [hep-ph]`.

[59] M. Bonvini, "Recent developments in small-x resummation," *Acta Phys. Polon. Supp.* **12** (2019) no. 4, 873, `arXiv:1812.01958 [hep-ph]`.

[60] J. Rojo, "Parton Distributions at a 100 TeV Hadron Collider," *PoS* **DIS2016** (2016) 275, `arXiv:1605.08302 [hep-ph]`.

[61] **IceCube** Collaboration, M. G. Aartsen *et al.*, "The IceCube Neutrino Observatory: Instrumentation and Online Systems," *JINST* **12** (2017) no. 03, P03012, `arXiv:1612.05093 [astro-ph.IM]`. [Erratum: JINST 19, E05001 (2024)].

[62] **KM3NeT** Collaboration, R. Coniglione, "The KM3NeT neutrino telescope," *J. Phys. Conf. Ser.* **632** (2015) 012002.

[63] L. A. Anchordoqui, "Ultra-High-Energy Cosmic Rays," *Phys. Rept.* **801** (2019) 1–93, `arXiv:1807.09645 [astro-ph.HE]`.

[64] J. Albrecht *et al.*, "The Muon Puzzle in cosmic-ray induced air showers and its connection to the Large Hadron Collider," *Astrophys. Space Sci.* **367** (2022) no. 3, 27, `arXiv:2105.06148 [astro-ph.HE]`.

[65] D. Soldin, "Astroparticle Physics with the Forward Physics Facility at the High-Luminosity LHC," *PoS* **ICRC2023** (2023) 327, `arXiv:2308.09079 [hep-ex]`.

[66] D. Soldin, "Astroparticle Physics at the Forward Physics Facility," in *58th Rencontres de Moriond on Very High Energy Phenomena in the Universe*. 7, 2024. `arXiv:2407.03427 [hep-ex]`.

[67] L. A. Anchordoqui, "Looking forward to forward physics at the CERN's LHC," *SciPost Phys. Proc.* **13** (2023) 042, `arXiv:2205.12413 [hep-ph]`.

[68] **Pierre Auger** Collaboration, A. Aab *et al.*, "Muons in Air Showers at the Pierre Auger Observatory: Mean Number in Highly Inclined Events," *Phys. Rev. D* **91** (2015) no. 3, 032003, `arXiv:1408.1421 [astro-ph.HE]`. [Erratum: Phys.Rev.D 91, 059901 (2015)].

[69] **Pierre Auger** Collaboration, A. Aab *et al.*, "Testing Hadronic Interactions at Ultrahigh Energies with Air Showers Measured by the Pierre Auger Observatory," *Phys. Rev. Lett.* **117** (2016) no. 19, 192001, `arXiv:1610.08509 [hep-ex]`.

[70] **Telescope Array** Collaboration, R. U. Abbasi *et al.*, "Study of muons from ultrahigh energy cosmic ray air showers measured with the Telescope Array experiment," *Phys. Rev. D* **98** (2018) no. 2, 022002, `arXiv:1804.03877 [astro-ph.HE]`.

[71] **EAS-MSU, IceCube, KASCADE-Grande, NEVOD-DECOR, Pierre Auger, SUGAR, Telescope Array, Yakutsk EAS Array** Collaboration, H. P. Dembinski *et al.*, "Report on Tests and Measurements of Hadronic Interaction Properties with Air Showers," *EPJ Web Conf.* **210** (2019) 02004, `arXiv:1902.08124 [astro-ph.HE]`.

[72] **EAS-MSU, IceCube, KASCADE-Grande, NEVOD-DECOR, Pierre Auger, SUGAR, Telescope Array, Yakutsk EAS Array** Collaboration, D. Soldin, "Update on the Combined Analysis of Muon Measurements from Nine Air Shower Experiments," *PoS* **ICRC2021** (2021) 349, `arXiv:2108.08341 [astro-ph.HE]`.

[73] **Pierre Auger** Collaboration, A. Abdul Halim *et al.*, "Testing hadronic-model predictions of depth of maximum of air-shower profiles and ground-particle signals using hybrid data of the Pierre Auger Observatory," *Phys. Rev. D* **109** (2024) no. 10, 102001, `arXiv:2401.10740 [astro-ph.HE]`.

[74] F. Riehn, R. Engel, A. Fedynitch, T. K. Gaisser, and T. Stanev, "Hadronic interaction model Sibyll 2.3d and extensive air showers," *Phys. Rev. D* **102** (2020) no. 6, 063002, `arXiv:1912.03300 [hep-ph]`.

[75] A. Fedynitch, F. Riehn, R. Engel, T. K. Gaisser, and T. Stanev, "Hadronic interaction model sibyll 2.3c and inclusive lepton fluxes," *Phys. Rev. D* **100** (2019) no. 10, 103018, `arXiv:1806.04140 [hep-ph]`.

[76] F. Riehn, A. Fedynitch, and R. Engel, "Sibyll*," *Astropart. Phys.* **160** (2024) 102964, `arXiv:2404.02636 [hep-ph]`.

[77] S. Ostapchenko, "QGSJET-II: physics, recent improvements, and results for air showers," *EPJ Web Conf.* **52** (2013) 02001.

[78] S. Ostapchenko, "Nonlinear screening effects in high energy hadronic interactions," *Phys. Rev. D* **74** (2006) no. 1, 014026, `arXiv:hep-ph/0505259`.

[79] S. Roesler, R. Engel, and J. Ranft, "The Monte Carlo event generator DPMJET-III," in *International Conference on Advanced Monte Carlo for Radiation Physics, Particle Transport Simulation and Applications (MC 2000)*, pp. 1033–1038. 12, 2000. `arXiv:hep-ph/0012252`.

[80] J. Allen and G. Farrar, "Testing models of new physics with UHE air shower observations," in *33rd International Cosmic Ray Conference*, p. 1182. 7, 2013. `arXiv:1307.7131 [astro-ph.HE]`.

[81] L. A. Anchordoqui, H. Goldberg, and T. J. Weiler, "Strange fireball as an explanation of the muon excess in Auger data," *Phys. Rev. D* **95** (2017) no. 6, 063005, `arXiv:1612.07328 [hep-ph]`.

[82] L. A. Anchordoqui, C. García Canal, S. J. Sciutto, and J. F. Soriano, "Through the looking-glass with ALICE into the quark-gluon plasma: A new test for hadronic interaction models used in air shower simulations," *Phys. Lett. B* **810** (2020) 135837, `arXiv:1907.09816 [hep-ph]`.

[83] L. A. Anchordoqui, C. G. Canal, F. Kling, S. J. Sciutto, and J. F. Soriano, "An explanation of the muon puzzle of ultrahigh-energy cosmic rays and the role of the Forward Physics Facility for model improvement," *JHEAp* **34** (2022) 19–32, `arXiv:2202.03095 [hep-ph]`.

[84] S. J. Sciutto, L. A. Anchordoqui, C. Garcia Canal, F. Kling, and J. F. Soriano, "Gauging the cosmic ray muon puzzle with the Forward Physics Facility," *PoS* **ICRC2023** (2023) 388, `arXiv:2307.08634 [hep-ph]`.

[85] S. J. Sciutto, "AIRES: A system for air shower simulations," `arXiv:astro-ph/9911331`.

[86] R. Gauld, J. Rojo, L. Rottoli, S. Sarkar, and J. Talbert, "The prompt atmospheric neutrino flux in the light of LHCb," *JHEP* **02** (2016) 130, `arXiv:1511.06346 [hep-ph]`.

[87] W. Bai, M. Diwan, M. V. Garzelli, Y. S. Jeong, K. Kumar, and M. H. Reno, "Forward production of prompt neutrinos from charm in the atmosphere and at high energy colliders," *JHEP* **10** (2023) 142, `arXiv:2212.07865 [hep-ph]`.

[88] W. Bai, M. Diwan, M. V. Garzelli, Y. S. Jeong, F. K. Kumar, and M. H. Reno, "Parton distribution function uncertainties in theoretical predictions for far-forward tau neutrinos at the Large Hadron Collider," *JHEP* **06** (2022) 148, `arXiv:2112.11605 [hep-ph]`.

[89] J. Boyd *et al.*, "Update on the FPF Facility technical studies." `https://cds.cern.ch/record/2851822`, 2023.

[90] J. Boyd *et al.*, "Update of Facility Technical Studies for the FPF." `https://cds.cern.ch/record/2904086`, 2024.

[91] D. Gamba *et al.*, "Impact of Vibration to HL-LHC Performance During the FPF Facility Construction." `https://cds.cern.ch/record/2901520`, 2024.

[92] "FLUKA." `https://fluka.cern`.

[93] **FASER** Collaboration, A. Ariga *et al.*, "Technical Proposal for FASER: ForwArd Search ExpeRiment at the LHC," `arXiv:1812.09139 [physics.ins-det]`.

[94] **SND@LHC** Collaboration, R. Albanese *et al.*, "Measurement of the muon flux at the SND@LHC experiment," *Eur. Phys. J. C* **84** (2024) no. 1, 90, `arXiv:2310.05536 [hep-ex]`.

[95] R. Garcia Alia, "Radiation safe level definition criteria for HL-LHC electronics," Tech. Rep. EDMS 2389056, 2021. `https://edms.cern.ch/document/2389056/1.1`.

[96] **FASER** Collaboration, H. Abreu *et al.*, "The FASER detector," *JINST* **19** (2024) no. 05, P05066, `arXiv:2207.11427 [physics.ins-det]`.

[97] **FASER** Collaboration, A. Ariga *et al.*, "FASER's physics reach for long-lived particles," *Phys. Rev. D* **99** (2019) no. 9, 095011, `arXiv:1811.12522 [hep-ph]`.

[98] **LHCb SciFi Tracker** Collaboration, P. Hopchev, "SciFi: A large Scintillating Fibre Tracker for LHCb," in *5th Large Hadron Collider Physics Conference*. 10, 2017. `arXiv:1710.08325 [physics.ins-det]`.

[99] K. Hennessy, "The LHCb Mighty Tracker," *PoS* **EPS-HEP2023** (2024) 565.

[100] S. Lee, M. Livan, and R. Wigmans, "Dual-Readout Calorimetry," *Rev. Mod. Phys.* **90** (2018) no. 2, 025002, `arXiv:1712.05494 [physics.ins-det]`.

[101] M. Antonello *et al.*, "Tests of a dual-readout fiber calorimeter with SiPM light sensors," *Nucl. Instrum. Meth. A* **899** (2018) 52–64, `arXiv:1805.03251 [physics.ins-det]`.

[102] F. Kling and S. Trojanowski, "Forward experiment sensitivity estimator for the LHC and future hadron colliders," *Phys. Rev. D* **104** (2021) no. 3, 035012, `arXiv:2105.07077 [hep-ph]`.

[103] S. Agostinelli *et al.*, "GEANT4 – a simulation toolkit," *Nucl. Instrum. Meth. A* **506** (2003) 250.

[104] X. Ai *et al.*, "A Common Tracking Software Project," *Comput. Softw. Big Sci.* **6** (2022) no. 1, 8, `arXiv:2106.13593 [physics.ins-det]`.

[105] **FASER** Collaboration, H. Abreu *et al.*, "Detecting and Studying High-Energy Collider Neutrinos with FASER at the LHC," *Eur. Phys. J. C* **80** (2020) no. 1, 61, `arXiv:1908.02310 [hep-ex]`.

[106] **FASER** Collaboration, H. Abreu *et al.*, "First neutrino interaction candidates at the LHC," *Phys. Rev. D* **104** (2021) no. 9, L091101, `arXiv:2105.06197 [hep-ex]`.

[107] A. Ariga, T. Ariga, G. De Lellis, A. Ereditato, and K. Niwa, *Nuclear Emulsions*, pp. 383–438. Springer International Publishing, 2020. `https://doi.org/10.1007/978-3-030-35318-6_9`.

[108] H. Rokujo, K. Sugimura, S. Yamamoto, H. Hayashi, M. Nakamura, Y. Nakamura, T. Nakano, O. Sato, and I. Usuda, "Nuclear emulsion film production system for experiments in full-area scanning and analysis era," *Nucl. Instrum. Meth. A* **1066** (2024) 169622.

[109] A. Haas, C. S. Hill, E. Izaguirre, and I. Yavin, "Looking for milli-charged particles with a new experiment at the LHC," *Phys. Lett. B* **746** (2015) 117–120, `arXiv:1410.6816 [hep-ph]`.

[110] A. Ball *et al.*, "A Letter of Intent to Install a milli-charged Particle Detector at LHC P5," `arXiv:1607.04669 [physics.ins-det]`.

[111] **milliQan** Collaboration, A. Ball *et al.*, "Sensitivity to millicharged particles in future proton-proton collisions at the LHC with the milliQan detector," *Phys. Rev. D* **104** (2021) no. 3, 032002, `arXiv:2104.07151 [hep-ex]`.

[112] "Eljen Technology." `https://eljentechnology.com/products/plastic-scintillators/ej-200-ej-204-ej-208-ej-212`, Accessed: Friday 8th November, 2024.

[113] "Saint-Gobain." `https://www.crystals.saint-gobain.com/products/bc-408-bc-412-bc-416`, Accessed: Friday 8th November, 2024.

[114] **milliQan** Collaboration, A. Ball *et al.*, "Search for millicharged particles in proton-proton collisions at $\sqrt{s} = 13$ TeV," *Phys. Rev. D* **102** (2020) no. 3, 032002, `arXiv:2005.06518 [hep-ex]`.

[115] M. Auger *et al.*, "The EXO-200 detector, part I: Detector design and construction," *JINST* **7** (2012) P05010, `arXiv:1202.2192 [physics.ins-det]`.

[116] D. A. Dwyer *et al.*, "LArPix: Demonstration of low-power 3D pixelated charge readout for liquid argon time projection chambers," *JINST* **13** (2018) no. 10, P10007, `arXiv:1808.02969 [physics.ins-det]`.

[117] N. Hoch *et al.*, "First operation of a multi-channel Q-Pix prototype: measuring transverse electron diffusion in a gas time projection chamber," *JINST* **19** (2024) no. 06, P06007, `arXiv:2402.05734 [hep-ex]`.

[118] A. Roberts *et al.*, "First demonstration of 3D optical readout of a TPC using a single photon sensitive Timepix3 based camera," *JINST* **14** (2019) no. 06, P06001, `arXiv:1810.09955 [physics.ins-det]`.

[119] A. Lowe, K. Majumdar, K. Mavrokoridis, B. Philippou, A. Roberts, C. Touramanis, and J. Vann, "Optical Readout of the ARIADNE LArTPC using a Timepix3-based Camera," *Instruments* **4** (2020) no. 4, 35, `arXiv:2011.02292 [physics.ins-det]`.

[120] A. J. Lowe *et al.*, "ARIADNE$^+$: Large Scale Demonstration of Fast Optical Readout for Dual-Phase LArTPCs at the CERN Neutrino Platform †," *Phys. Sci. Forum* **8** (2023) no. 1, 46, `arXiv:2301.02530 [physics.ins-det]`.

[121] **Baby MIND** Collaboration, S.-P. Hallsjö, "Baby MIND: A magnetised spectrometer for the WAGASCI experiment," *PoS* **NuFact2017** (2018) 078.

[122] G. Rolando, P. Benoit, A. Blondel, A. Dudarev, E. Noah, H. Pais Da Silva, M. Rayner, and H. H. J. ten Kate, "New and Optimized Magnetization Scheme for the Baby Magnetized Iron Neutrino Detector at J-PARC," *IEEE Trans. Magnetics* **53** (2017) no. 5, 8000706.

[123] **FASER** Collaboration, H. Abreu *et al.*, "Search for dark photons with the FASER detector at the LHC," *Phys. Lett. B* **848** (2024) 138378, `arXiv:2308.05587 [hep-ex]`.

[124] **FASER** Collaboration, R. Mammen Abraham *et al.*, "Shining Light on the Dark Sector: Search for Axion-like Particles and Other New Physics in Photonic Final States with FASER," `arXiv:2410.10363 [hep-ex]`.

[125] "FASER." `https://faser.web.cern.ch`.

[126] "milliQan." `https://u.osu.edu/milliqan`.

[127] L. A. Anchordoqui *et al.*, " Forward Physics Facility," *BNL-224243-2023-COPA* (2023) , `OSTI:1972463`.

[128] P. Christensen, L. Dysert, J. Bates, D. Burton, R. Creese, and J. Hollmann, "18-R-97 Cost Estimate Classification System – as applied in engineering, procurement, and construction for the process industries,". 2016.